ARKIV FÖR FYSIK Band 15 nr 27

Communicated 11 February 1959 by Manne Siegbahn and Erik Hulthén

# A study of the photoelectric effect and its application to the determination of gamma-ray intensities

By Sölve Hultberg

With 16 figures in the text

## Contents

A. Historical review of experimental work . . . . . . . . . . . . . . . . 308
B. Theoretical treatment of the photoelectric effect . . . . . . . . . . . 310
C. Discussion of the experimental method . . . . . . . . . . . . . . . . . 317
D. Experimental procedure and results . . . . . . . . . . . . . . . . . . 318
E. The experimental distribution function and its properties . . . . . . . . 324
F. Theory and experiment . . . . . . . . . . . . . . . . . . . . . . . . 332
G. The relative photoelectric absorption of gamma-rays by the electron shells of the uranium atom. A discussion of the accuracy of available photoelectric cross-sections for $Z=92$ . . . . . . . . . . . . . . . . . . . . . 334
H. The application of the photoelectric effect to the determination of gamma-ray intensities. The source–converter geometry . . . . . . . . . . . . 338
I. Remarks and conclusions . . . . . . . . . . . . . . . . . . . . . . . 349

## Introduction

It is the object of the present paper to give a detailed account of a series of beta-spectrometric experiments, aiming at a study of the particular type of interaction between gamma-radiation and matter which is commonly described as the photoelectric effect. Due to the action of the electromagnetic radiation this phenomenon results in the emission of an atomic electron from a bound state, with the simultaneous disappearance of the radiation quantum which spends itself completely in liberating the electron and giving it kinetic energy. Particles obtained by processes of this kind are called photoelectrons.

Earlier experimental and theoretical work on the properties of the photoelectric emission was particuarly intense about 30 years ago. Since then, interest in this field of research whose problems were far from solved, has been rather small on account of experimental and theoretical difficulties. However, with the rapid development, during the last fifteen years, of the technique of beta-spectroscopy, interest in a better understanding of the characteristics of the photoeffect has been revived, due to the increasing need of more precise information about gamma-ray intensities. The photoelectric method for the determination of gamma-ray intensities is a very attractive one, for it permits a resolution comparable to that possible in internal conversion work, and in this respect it is superior to other methods. This is obviously of particular value in cases of complex spectra.

The purpose of the investigation reported here was twofold: (*a*) A study of the properties of the longitudinal angular dependence of the photoelectric effect, and (*b*) an application of the results of such a study to a general and practical analysis of photolines, for the correct determination of gamma-ray intensities.

It should be noted that no systematic investigation of the photoelectric effect in the sense of point (*a*) has ever been carried out in the beta-spectroscopically important energy region 100–2000 keV. This patent lack in our experimental knowledge about one of the fundamental processes by which electromagnetic radiation is absorbed in matter, constitutes in itself a strong reason for starting an investigation. It should also be noted that a successful solution of the problem stated in point (*b*), should permit, in particular, a technique leading to an unconditional beta-spectrometric determination of *absolute* values of photoelectric cross-sections and internal conversion coefficients.

## A. Historical review of experimental work

### *The nature of the photoelectric effect*

Shortly after the discovery of the X-rays it was found that a type of short-range secondary radiation was produced when such rays were allowed to fall on solid screens. By deflection experiments in a magnetic field Dorn was able to show in 1900 that this secondary radiation consisted of negatively charged particles (electrons). In the early experiments the ionization produced in a gas by the particles was measured. Later the cloud chamber became the most frequently used instrument in the study of the photoelectric effect because it allowed a study of the number of the electrons emitted, of the spatial distribution and shape of their tracks, and of their range in air. Experiments in the early twenties showed that the electrons in question all had an energy, slightly less than the quantum energy $h\nu$, in accordance with Einstein's photoelectric equation

$$h\nu = E_{\text{kin}} + \omega,$$

where $E_{\text{kin}}$ is the kinetic energy of the ejected electron and where $\omega$ is the liberation energy. Electrons obtained in processes described by Einstein's equation are generally called photoelectrons. Experiments in 1921 by de Broglie and by Simons in the X-ray region and by Ellis in the gamma-ray region finally established the existence of groups of photoelectrons with different velocities (for every particular $h\nu$ value), corresponding to their origin from different parts of the atom. $\omega$ was thus to be interpreted as the binding energy of the respective shell from which the electron was emitted. It was then possible to use the above equation in the reverse sense, i.e. gamma-ray energies could be inferred from a determination of the velocities of photoelectrons in magnetic analyzers.

### *The spatial distribution of the photoelectric emission*

In 1912 Cooksey showed that the number of photoelectrons produced from thin metallic foils by the action of X-rays was greater on the side of emergence of the X-rays than on the side of incidence. The first results, for unpolarized X-rays, about the detailed character of the photoelectric angular distribution in a plane containing the propagation direction of the X-rays (defining the longitudinal or $\theta$-dependence, where the incidence direction of the quanta is represented as $\theta = 0^\circ$) were obtained in 1924 by Bothe with a GM-counter in a specially constructed chamber for experiments with gases. Most of the electrons were found to be ejected nearly perpendicularly to the direction $\theta = 0^\circ$, and it was possible to define an angle $\theta_m$ for which the photoelectric emission reached a maximum. In 1924 Bubb studied polarized X-rays with a cloud chamber and investigated the angular distribution in a plane perpendicular to the direction $\theta = 0^\circ$ (defining the azimuthal or $\varphi$-dependence, where the direction of the electric vector is represented as $\varphi = 0^\circ$). He observed that the direction of the electric vector of the electromagnetic radiation is strongly preferred and found two sharp maxima in the positive and negative directions of the electric vector. The $\varphi$-dependence was found to be independent of energy while this was not the case with the $\theta$-dependence.

The most detailed investigation of the $\theta$-distribution was performed by Watson and coworkers in 1927–31. They used a magnetic spectrometer of a somewhat special type allowing photoelectrons, emitted from thin metal foils, to be studied under any angle of emergence $\theta$, with $\theta = 0^\circ$ defined as above. The magnetic analysis permitted a separation of the photoelectrons from the $K$, $L_\mathrm{I}$, $L_\mathrm{II}$, ... shells. A few settings of the angle $\theta$ were investigated for every shell using a photographic plate and, later, a GM-counter for detection.

Several other investigators worked in the years 1924–31 with these problems both experimentally and theoretically. A detailed account of the works carried out before 1928 is to be found in the comprehensive article by Kirchner (1930). Most of the experimenters used cloud chambers because of the visualization of the events. At the beginning of the thirties the interest in the study of the properties of the photoelectrons rapidly diminished, and during the last 25 years very few experiments in this field have been undertaken (cf. Eggleston and Martin, 1936). The main reason for this decline in interest seems to have been the lack of such fields of application of the photoelectric process where a detailed knowledge about the phenomenon was urgently required. With the rapid development of beta-spectroscopy after the second world war, interest in extended and more accurate information on the longitudinal angular dependence revived, because a beta-spectrometric study of photolines could be expected to give the most accurate information about gamma-ray intensities. In 1947 Latyshev carried out a beta-spectrometer measurement of the $\theta$-distribution of 2.6 MeV photoelectrons, ejected from a thin Th foil, and in 1952 Hedgran made a similar experiment at $h\nu = 412$ keV (using a thin uranium converter). Hereford (1951) and Hereford and Keuper (1953) investigated the $\varphi$-dependence with a scintillation counter arrangement, using annihilation radiation. The first systematic study in the gamma-ray region of the $\theta$-distribution was carried out by Hedgran and Hultberg (1954) and Hultberg (1955), and the present paper will give a full account of extended and more careful measurements at $h\nu = 412$, 662 and 1332 keV.

It should be added that that the $\theta$-distribution has never been studied using *polarized* X- or gamma-rays. It may also be noted that only the $\theta$-dependence is of any practical importance and, for this reason, no attention has been paid, in the present investigation, to the $\varphi$-dependence.

## B. Theoretical treatment of the photoelectric effect

In this section we will give a brief outline of the present state of the theory for the anisotropy of the photoelectric effect and indicate expressions of some quantities, useful for the experimental comparison.

### *The angular dependence*

Consider an electromagnetic field of field strengths **E** and **H**. The force acting on an electric charge $e$, moving in the field, can be written, non-relativistically, (Heitler, § 1)

$$m\,d\mathbf{v}/dt = e[\mathbf{E} + c^{-1}(\mathbf{v}\times\mathbf{H})], \tag{1}$$

where $m$ is the rest mass of the charge. However, for many applications it is more convenient to express the Newtonian equation of motion (1) with the help of a function $H$ of the $2n$ coordinates and momenta $H = H(x_1, x_2, \ldots, x_n; p_1, p_2, \ldots, p_n)$. $H$ is identical with the Hamiltonian function when it satisfies the $2n$ canonical relations

$$dx_i/dt = \partial H/\partial p_i, \qquad dp_i/dt = -\partial H/\partial x_i. \tag{2}$$

In the non-relativistic limit it is not difficult to show that Eqs. (1) and (2) are identical if the function $H$ is written (Becker, §§ 12 and 64)

$$H = \frac{1}{2m}\left(\mathbf{p} - \frac{e}{c}\mathbf{A}\right)^2 + e\varphi. \tag{3}$$

**A** and $\varphi$ are the vector and scalar potentials, defining the electromagnetic field, according to

$$\mathbf{E} = -\operatorname{grad}\varphi - \frac{1}{c}\frac{\partial\mathbf{A}}{\partial t}; \qquad \mathbf{H} = \operatorname{rot}\mathbf{A}. \tag{4}$$

If, moreover, the charged particle experiences a force due to an additional potential energy $V$, the Hamiltonian becomes (Schiff, § 23)

$$H = \frac{\mathbf{p}^2}{2m} - \frac{e}{2mc}(\mathbf{A}\,\mathbf{p} + \mathbf{p}\,\mathbf{A}) + \frac{e^2}{2mc^2}\mathbf{A}^2 + e\varphi + V. \tag{5}$$

Any function $\mathbf{f}(\mathbf{r})$ obeys the commutation relation $[\mathbf{f}, \mathbf{p}] = \mathbf{f}\,\mathbf{p} - \mathbf{p}\,\mathbf{f} = i\hbar\operatorname{div}\mathbf{f}$ and, consequently, $[\mathbf{A}, \mathbf{p}] = \mathbf{A}\,\mathbf{p} - \mathbf{p}\,\mathbf{A} = \mathrm{i}\cdot\hbar\operatorname{div}\mathbf{A}$. Thus, equation (5) becomes

$$H = \frac{\mathbf{p}^2}{2m} - \frac{e}{mc}\mathbf{A}\,\mathbf{p} + \frac{ie\hbar}{2mc}\operatorname{div}\mathbf{A} + \frac{e^2}{2mc^2}\mathbf{A}^2 + e\varphi + V \tag{6}$$

and, introducing conventional operator notations, we obtain the Schrödinger equation as

$$i\hbar\partial\psi/\partial t = \left(-\frac{\hbar^2}{2m}\nabla^2 + \frac{ie\hbar}{mc}\mathbf{A}\operatorname{grad} + \frac{ie\hbar}{2mc}\operatorname{div}\mathbf{A} + \frac{e^2}{2mc^2}\mathbf{A}^2 + e\varphi + V\right)\psi\cdot \tag{7}$$

For the simplification of Eq. (7) it should be observed that Eqs. (4) do not define the potentials A and $\varphi$ uniquely. Because of the general vector relation rot grad $x = 0$ it is obvious that A and $\varphi$ can be replaced by new potentials A′ and $\varphi'$, according to

$$\mathbf{A}' = \mathbf{A} + \operatorname{grad} \chi \quad \text{and} \quad \varphi' = \varphi - \frac{1}{c}\frac{\partial \chi}{\partial t}.$$

The possible conventions for choosing A′ and $\varphi'$, without changing **E** and **H**, are called *gauges* and the invariance of **E** and **H** under such transformations is called *gauge invariance*. Two types of gauges are commonly used, namely the Lorentz and the Coulomb gauges, according to the conditions $\operatorname{div} \mathbf{A}' + (1/c)(\partial\varphi'/\partial t) = 0$ and $\operatorname{div} \mathbf{A}' = 0$, respectively (Heitler, § 1). As we are here working with the field in free space (no charges), the gauge function $\chi$ can be chosen within the Lorentz gauge so that the scalar field $\varphi$ vanishes, e.g.

$$\operatorname{div} \mathbf{A} = 0, \qquad \varphi = 0, \tag{8}$$

where, for convenience, the primes have been dropped. Inserting the field strengths, expressed in the vector A, into the Maxwell equations we obtain a differential equation for A

$$\nabla^2 \mathbf{A} - \frac{1}{c^2}\frac{\partial^2 \mathbf{A}}{\partial t^2} = 0, \tag{9}$$

which admits transverse plane wave solutions for A and hence for **E** and **H**. We can write (Schiff, § 35)

$$\mathbf{A}(\mathbf{r}, t) = \mathbf{A}_0 e^{i(\mathbf{kr} - \omega t)} + \text{complex conjugate}. \tag{10}$$

**k** is the propagation vector of the electromagnetic wave and $\mathbf{A}_0$ is the polarization vector, perpendicular to **k**.

On account of (8) the number of terms in Eq. (7) is reduced. Moreover, on the right-hand side, the fourth term is small compared with the second, and the latter is, in turn, small compared with the first term, the ratios being of the order of $eA/(cp)$ in both cases. The magnitude of the latter quantity is small in practice and thus, to a first-order approximation, the term $e^2A^2/(2mc^2)$ can be neglected in a perturbation treatment of Eq. (7) which, consequently, can be written (Schiff, § 35)

$$i\hbar\,\partial\psi/\partial t = (H^0 + H')\psi \tag{11}$$

with

$$\left.\begin{aligned} H^0 &= -\frac{\hbar^2}{2m}\nabla^2 + V, \\ H' &= \frac{ie\hbar}{mc}\mathbf{A}\operatorname{grad}. \end{aligned}\right\} \tag{12}$$

The emission and absorption of radiation quanta by an atom can be treated with Eqs. (11) and (12). The atom and the radiation form two quantum-mechanical systems which interact through the term $H'$, regarded as a perturbation. This interaction will produce transitions of the unperturbed system, resulting in the transition of the atom from one state to another and of an absorption or emission of light quanta.

In order to obtain an expression of the transition probability per unit time for the absorption of light quanta (photoeffect) we expand the wave function $\psi$ in the eigenfunctions $\psi^0$ of the unperturbed, time-independent wave equation, according to $\psi(t)=\sum_n a_n(t)\,\psi_n^0$, where the coefficients depend upon the time. $|a_n(t)|^2$ gives the probability for the system to be in the unperturbed state $n$ at time $t$. $1/t\,|a_f(t)|^2$ represents the transition probability per unit time for the transition from the initial state $i$ to the final state $n=f$, according to (Heitler, § 14)

$$\frac{1}{t}\left|a_f(t)\right|^2=\frac{2\pi}{\hbar}\left|H'_{fi}\right|^2\delta(E_f-E_i). \tag{13}$$

The Dirac function $\delta(E_f-E_i)$ represents the conservation of energy; only transitions between states of equal unperturbed energy can take place. Eq. (13) has a definite meaning only if an integration over either $E_f$ or $E_i$ can be carried out, meaning that one of the states must belong to a domain with energy values having an infinitely close spacing, i.e. a continuum. If $\varrho_f$ denotes the density of final electron states $f$ with energy $E_f$ we finally obtain, for the total transition probability $w_{fi}$,

$$w_{fi}=\frac{1}{t}\int\left|a_f(t)\right|^2\varrho_f\,d\,E_f=\frac{2\pi}{\hbar}\left|H'_{fi}\right|^2\varrho_f, \tag{14}$$

where

$$H'_{fi}\sim\int\psi_f^*\,\mathbf{A}\,\mathrm{grad}\,\psi_i. \tag{15}$$

In (15) a proportionality factor has been omitted, for simplicity. We assume that the system is initially in the state $i$ and that the perturbation is turned on at $t=0$. An introduction of (10) into (15) then gives for the *absorption* process

$$H'_{fi}\sim\int\psi_f^*\,e^{i\mathbf{kr}}\,\mathrm{grad}_A\,\psi_i, \tag{16}$$

where $\mathrm{grad}_A$ denotes the component of grad in the direction of $\mathbf{A}_0$. It might be observed that $e^{i\mathbf{kr}}$ commutes with $\mathrm{grad}_A$ because $\mathbf{A}_0$ and $\mathbf{k}$ are perpendicular.

The interpretation of Eq. (14) for the case of the $K$-shell photoelectric absorption of light quanta means that, in formula (16), $\psi_i$ is to be identified with the wave function of the electron in the $K$-shell and $\psi_f$ with the wave function of the electron in the continuum. We can write (Heitler, § 21)

$$\psi_i\sim e^{-r/a},\qquad \psi_f=e^{i\mathbf{pr}/\hbar}, \tag{17}$$

where $\mathbf{p}$ is the momentum of the electron and $a\cdot Z=a_0$ is the Bohr radius. Putting $\mathbf{u}=\hbar\,\mathbf{k}$ we then obtain for $H'$

$$H'\sim\int e^{-i\mathbf{pr}/\hbar}\,e^{i\mathbf{ur}/\hbar}\,\mathrm{grad}_A\,e^{-r/a}$$

$$=\int e^{i\mathbf{qr}/\hbar}\,\mathrm{grad}_A\,e^{-r/a}, \tag{18}$$

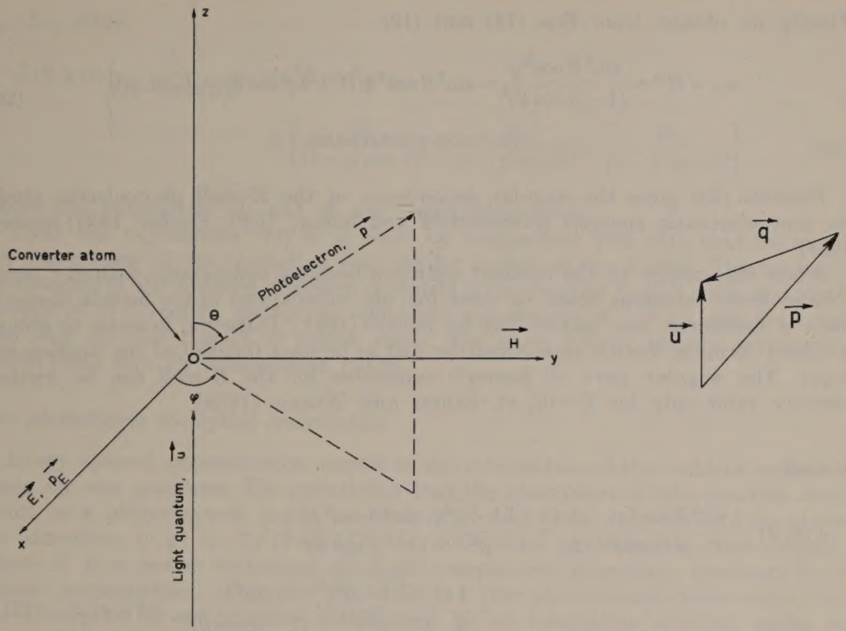

Fig. 1. The photoelectric emission, defined in spherical polar coordinates. **E** and **H** are the electric and magnetic vectors of a light quantum, which is incident along the $z$-axis.

where $\mathbf{q}=\mathbf{u}-\mathbf{p}$ is the momentum transferred to the atom. Carrying out the integration, Eq. (18) becomes, after squaring $H'$, (Heitler, § 21)

$$H'^2 \sim p_E^2/(\alpha^2+q^2)^4, \tag{19}$$

neglecting the proportionality factor. $\mathbf{p}_E$ is the component, along the direction of the electric vector, of the electron momentum (Fig. 1). $\alpha=\hbar Z/a_0=mZ/137=\sqrt{2mI}=$ momentum of the electron in the bound state ($I=$ ionization energy).

In order to derive the angular dependence, which enters the transition probability $w$ through $H'$, we consider the specific coordinate system in Fig. 1 *a*. The vector $\mathbf{u}$ is directed along the $z$-axis, $\mathbf{p}_E$ along the $x$-axis and $\mathbf{p}$ along the emission direction $(\theta,\varphi)$ of the photoelectron. The resulting momentum $\mathbf{q}$ of the atom can thus be written

$$q^2=p^2+u^2-2pu\cos\theta.$$

Furthermore, $p_E=p\sin\theta\cos\varphi$ and $\alpha^2+p^2=2m(I+E_{\text{kin}})=2mh\nu=2muc$. In the non-relativistic limit we have $u=h\nu/c \ll mc$ and hence

$$\begin{aligned}\alpha^2+q^2&=\alpha^2+p^2+u^2-2pu\cos\theta=2mcu+u^2-2pu\cos\theta\\&=u(2mc+u-2p\cos\theta)\sim 2mcu\,(1-\beta\cos\theta)\quad(\beta=v/c=p/(mc)).\end{aligned}$$

Finally we obtain, from Eqs. (14) and (19),

$$\left.\begin{aligned} w_{fi} \sim H'^2 \sim \frac{\sin^2\theta\cos^2\varphi}{(1-\beta\cos\theta)^4} \sim \sin^2\theta\cos^2\varphi\,(1+4\beta\cos\theta) = J_n(\theta,\varphi) \\ (n = \text{non-relativistic}). \end{aligned}\right\} \qquad (20)$$

Formula (20) gives the angular dependence of the $K$-shell photoelectric effect for non-relativistic energies (Sommerfeld and Schur, 1930; Fischer, 1931; Sauter, 1931).

When the energy of the incident quantum becomes comparable with $mc^2$, relativistic wave functions must be used for the calculations of the matrix element. Such a treatment was carried out by Sauter (1931). However, in order to obtain a closed formula Born's approximation had to be used (neglect of the binding energy). The angular part of Sauter's expression for the *K-shell* can be written (strictly valid only for $Z=0$), cf. Sauter and Wüster (1955),

*K-shell:*

$$J(\theta,\varphi) = \frac{\sin^2\theta\cos^2\varphi}{(1-\beta\cos\theta)^4} - \frac{1}{2}\,\frac{(1-\sqrt{1-\beta^2})}{1-\beta^2}\,\frac{\sin^2\theta\cos^2\varphi}{(1-\beta\cos\theta)^3} + \frac{1}{4}\,\frac{(1-\sqrt{1-\beta^2})^2}{(1-\beta^2)^{3/2}}\,\frac{\sin^2\theta}{(1-\beta\cos\theta)^3} \quad (\beta = v/c). \qquad (21)$$[1]

The structures of the formulae (20) and (21) are similar; the two last terms of (21) are small and can be regarded as relativistic corrections to the first term which is identical with (20). In practice, polarized electromagnetic radiation is never used and then Eq. (21) can immediately be integrated over all angles $\varphi$, giving

$$\left.\begin{aligned} J(\theta) = \frac{\sin^2\theta}{(1-\beta\cos\theta)^4} + \frac{1}{2}\,\frac{3(1-\sqrt{1-\beta^2})-2\beta^2}{(1-\beta^2)^{3/2}}\,\frac{\sin^2\theta}{(1-\beta\cos\theta)^3} = J_n(\theta) + c(\beta)\,J_r(\theta) \\ (n = \text{non-relativistic}, \quad r = \text{relativistic}). \end{aligned}\right\} \qquad (22)$$

An introduction of the appropiate wave functions for the bound states into (16) permits the calculation of the angular functions for higher shells (Hall, 1936). In the *non*-relativistic limit the $L$-shell splits into two groups with different wave functions, namely $L_{\mathrm{I}}$ ($s$-electrons) and $L_{\mathrm{II}}$–$L_{\mathrm{III}}$ ($p$-electrons). Accordingly, we obtain (Sommerfeld, VI:6)

*$L_{\mathrm{I}}$-shell:*

$$J(\theta,\varphi) = \sin^2\theta\cos^2\varphi\left[\frac{A_1}{(1-\beta\cos\theta)^4} + \frac{A_2}{(1-\beta\cos\theta)^5} + \frac{A_3}{(1-\beta\cos\theta)^6}\right];$$

---

[1] An expression of a largely similar character was recently obtained by H. Banerjee (1958). For more details, see section E.

*$L_{II}$–$L_{III}$ shells:*

$$J(\theta,\varphi)=\frac{1}{(1-\beta\cos\theta)^2}+\sin^2\theta\cos^2\varphi\times$$
$$\times\left[\frac{B_1}{(1-\beta\cos\theta)^4}+\frac{B_2}{(1-\beta\cos\theta)^5}+\frac{B_3}{(1-\beta\cos\theta)^6}\right], \tag{23}$$

where the parameters $A_\nu$ and $B_\nu$ are angle-independent.

From the expressions (23) it is seen, by comparison with (21), that the angular dependence of the $L$-shell is very similar to that of the $K$-shell. The tendency for ejection in the forward direction is clearly larger for the $L$-shell (fifth and sixth powers of $(1-\beta\cos\theta)$. So far, no *relativistic* calculations of $J(\theta,\varphi)$ have been carried out for the $L$-shell or higher shells. For more details, see the articles by Hall (1936) and by Sommerfeld (1939).

### *The photoelectric absorption cross-section*

Every ejected photoelectron results in the attenuation of the incident radiation beam by one quantum. The probability that the absorption of this quantum shall result in a photoelectron inside an element of solid angle $d\Omega=\sin\theta\,d\theta\,d\varphi$ about the direction $(\theta,\varphi)$ is $N J(\theta,\varphi)\,d\Omega$ (the differential photoelectric cross-section), where $N$ is a factor containing all angle-independent quantities, necessary for a correct normalization. The *total* probability $\tau$ (the photoelectric cross-section) for the absorption of one quantum is obtained by an integration over all angles as

$$\tau=\int N J(\theta,\varphi)\,d\Omega=2\pi N\int_0^\pi J(\theta)\sin\theta\,d\theta \tag{24}$$

which applies to a specific atomic shell, characterized by $J(\theta,\varphi)$. The shell in question is usually indicated by subscripts, as $\tau_K, \tau_L, \ldots, \tau_a$; the last subscript indicates an absorption due to the *whole* atom, i.e. the sum of the probabilities for all shells.

In order to obtain $\tau$ it is not necessary to evaluate $J(\theta,\varphi)$ and integrate over all angles, in the sense of Eq. (24). It is easier to calculate $\tau$ directly, and thus $\tau$ has been the object of a number of theoretical studies. However, due to extremely heavy mathematical analysis it is probably not possible to derive a practical formula for $\tau$, covering all $Z$-values and all energies of experimental interest. For details regarding available expressions for $\tau$, see the surveys given by Hall (1936), Davisson (1955) and White (1957).

### *Formulas for comparison with experiment*

For the experimental test of the theory of the photoeffect two principal methods can be followed. The first one consists of a determination of $\tau$ (not implying any knowledge of the differential cross-section) and the second is a direct study of the character of $J(\theta)$. The argument $\varphi$ will be omitted in the following text because only the $\theta$-dependence is of any practical interest. The latter alternative is difficult but should be more satisfactory, as it allows a detailed comparison with theory.

Depending upon the type of experiment the comparison of the $\theta$-function with theory may be based on one or several of the following conventional quantities (Davisson and Evans, 1952):

1. the plot of the angular function $J(\theta)$;
2. the "asymmetry" ratio $Q$ of the number of photoelectrons emitted in a *forward* direction ($0^\circ < \theta < 90^\circ$) to the number of those emitted in a *backward* direction ($90^\circ < \theta < 180^\circ$),

$$Q = \frac{\int_0^{\frac{1}{2}\pi} J(\theta) \sin\theta \, d\theta}{\int_{\frac{1}{2}\pi}^{\pi} J(\theta) \sin\theta \, d\theta}; \tag{25}$$

3. the "bipartition" angle $\theta_b$, i.e. the half-angle of a cone such that half of all the photoelectrons are emitted within this cone,

$$\int_0^{\theta_b} J(\theta) \sin\theta \, d\theta = \int_{\theta_b}^{\pi} J(\theta) \sin\theta \, d\theta; \tag{26}$$

4. the *average* value of $\cos\theta$ which is intimately related to the ratio $R$ of the average forward momentum of the photoelectrons to the momentum of the incident photon,

$$\overline{\cos\theta} = \frac{\int_0^{\pi} J(\theta) \sin\theta \cos\theta \, d\theta}{\int_0^{\pi} J(\theta) \sin\theta \, d\theta} \tag{27}$$

$$R = \frac{h\nu - \omega}{h\nu} \sqrt{1 + \frac{2mc^2}{h\nu - \omega}} \; \overline{\cos\theta}, \tag{28}$$

($m$ = rest mass of the electron).

In (27) $\omega$ denotes the binding energy of the respective shell. $R$ was given in the above form by Hultberg and Novakov (1957). The quantities $Q$ and $\theta_b$ are conveniently determined from plots of

$$T(\theta) = \frac{\int_0^{\theta} J(\theta) \sin\theta \, d\theta}{\int_0^{\pi} J(\theta) \sin\theta \, d\theta} \qquad (0 < \theta < \pi). \tag{29}$$

$Q$ is obtained as $T(\frac{1}{2}\pi)/[T(\pi) - T(\frac{1}{2}\pi)]$, and $\theta_b$ is the angle for which $T(\theta_b) = \frac{1}{2}$.

## C. Discussion of experimental methods

In section B, p. 315, it was remarked that the most satisfactory method for testing the theory of the photoeffect would be a detailed study of the properties of the function $N J(\theta)$, for the different atomic shells. As is evident from section A, two types of instrument have been used: the cloud chamber and the magnetic analyzer (beta-spectrometer). The main drawbacks of the former apparatus is the formidable work associated with the analysis of the recorded tracks. For practical reasons, this circumstance heavily limits the statistics; usually some 400–500 tracks are being observed, from which the whole function $J(\theta)$ is to be derived (for details about the experimental technique of the cloud chamber, see Eggleston and Martin, 1937). Obviously, a direct comparison of the forms of the theoretical and experimental functions is difficult here; it is usually better to make a comparison on the basis of the quantities $Q, \theta_b$, $\overline{\cos\theta}$, $R$ or/and $T$, Eqs. (25)–(29).

The beta-spectrometric method was originally applied by Watson (1927), who made a special construction for the purpose. However, only very few points (5–6) were recorded on each distribution, permitting only a rough check on the theory (the measurements were carried out for energies below 100 keV). In 1947 Latyshev showed that the distribution could be studied in an ordinary beta-spectrometer and that it was possible to work with high energies (his gamma-ray energy was 2.6 MeV). Finally, Hedgran (1952) used a similar technique in a double-focusing beta-spectrometer at an energy of 412 keV. It should be observed that only the two latter workers were able to give reasonably satisfactory representations of their results, in the form of plots of the angular functions. Their plots were, however, *incomplete*, in that they covered only part of the angular interval. The first *complete* beta-spectrometric measurements of photoelectric distributions were carried out by Hultberg and Novakov (1957) who were able to represent the angular functions for all angles $\theta$.

Because of the good statistics and the relatively simple experimental set-up it was considered worthwhile to examine the spectrometer method more closely than was done by Latyshev and by Hedgran. In the latter works no attempts were made towards an analysis of the obtained distribution curves $J_e(\theta)$ (the subscript $e$ indicates *experimental*), since the study of the photoeffect was not the main purpose of these investigations. Moreover, no distribution curves have ever been presented showing the $\theta$-dependence of higher shells (the scanty evidence in very small parts of the angular range and at low energies, obtained by Watson and coworkers, is disregarded). Also, it should be observed that the angular dependence of the photoeletrons plays a fundamental role in the analysis of photolines for the deduction of gamma-ray intensities (Hultberg and Stockendal, 1959 *a*). A knowledge of correlated $\theta$-functions for all atomic shells would also permit a determination of the absorption ratios of the various shells, giving better possibilities of obtaining experimental values of the photoelectric cross-section $\tau_K$ and, indirectly, of the pair production cross-section. Finally, if the true function $J(\theta)$ can be deduced from $J_e(\theta)$, a close test of the theory of the photoeffect would be possible.

The following section will give a detailed account of the experimental procedure followed, in order to extend the measurements reported by Hedgran and Hultberg (1954) and Hultberg (1955).

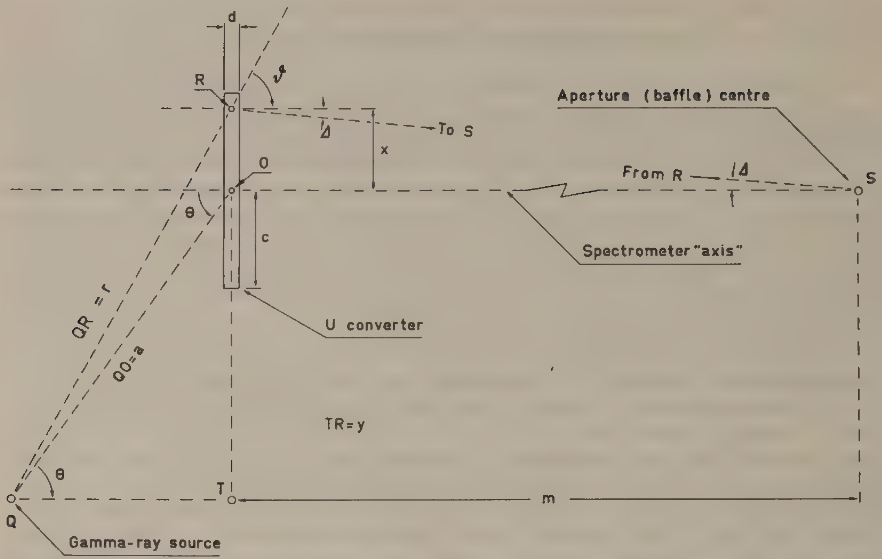

Fig. 2. Schematic illustration of the experimental set-up inside the spectrometer. The gamma-ray source is at $Q$, the converter centre at $O$ and the baffle centre at $S$. The converter is circular.

## D. Experimental procedure and results

In the following text we will frequently use the simplified notation $M'$ in order to indicate the sum effect of the $M, N, O, \ldots$ atomic shells.

The distribution function $J(\theta)$ was studied for the $K$, $L$, and $M'$ shells at the gamma-ray energies 412, 662 and 1332 keV (Hultberg and Sujkowski, to be published), using a double-focusing spectrometer of 50 cm mean radius. Fig. 2 illustrates, schematically, the experimental arrangement inside the spectrometer, at the ordinary source position.

Principally, it is natural to regard the incidence direction of the quanta as fixed and the emission direction $\theta$ of the photoelectrons as variable. In the spectrometer experiments, however, it is necessary to take the reverse point of view; here the emission direction through the baffle centre is fixed and the radiation has to take different directions of incidence $\theta$. Such an arrangement also has the advantage that the recorded photoelectrons always emerge nearly perpendicularly to the converter surface, implying a minimization of the influence of scattering on the electron paths through the converter material (cf. below).

Throughout the measurements uranium was used for the transformation of the radiation quanta into electrons, i.e. as *converter* or *radiator* material. Because it is essential that the converter have a good uniformity over the entire surface a very careful preparation of uranium foils was undertaken, following the painting method of Glover and Borrell (1955). In this way five rectangular foils (area 63 cm$^2$) on 0.1 mm aluminium backings were prepared (Novakov *et al.*, 1958).

The homogeneity was tested by studying the blackening of X-ray films, placed in direct contact with the uranium, and by carrying out accurate determinations of the uranium content at different parts of the same foil (the quantitative analyses were performed by AB Atomenergi, Stockholm; cf. Hultberg and Stockendal, 1959 *a*). It was concluded that the overall homegeneity of any of the foils was better than 3%. By studying photometer recordings of the X-ray film blackenings small circular foils could be punched out, having a homogeneity better than 1%. In order to depress the continuous background during the measurements the material around the converter was minimized by mounting the respective foil on a thin aluminium wire (diameter 2 mm, length 40 mm, Fig. 3 *b*). If not otherwise stated the diameter of all converters used was 14.6 mm.

The gamma-rays were obtained from reactor-produced activities of the isotopes $Au^{198}$, $Cs^{137}$ and $Co^{60}$. They were contained in the A.E.R.E., Harwell, standard aluminium capsules for radiographic sources, of the $2 \times 2$ mm size. The source strengths were 250–300 mC.

In order to realize different values of the relative angle $\theta$ the particular radiation source was placed in a vertical aluminium holder which could be rotated in a horizontal plane (the plane of the central electron orbit), with the middle $O$ of the converter as the centre (Fig. 2). For convenience, a special construction was made, permitting an easy operation, i.e. the angle $\theta$ and the distance $a$ could be set from outside the spectrometer. This is of special importance considering the relatively short half-life of $Au^{198}$ and the requirements of radiation protection. The mechanical constructions are shown in Fig. 3.

The source holder is mounted on a sliding rod, consisting of two identical parts, one of which has vertical cogs on the inside, in order to make the radial movement possible. The whole rod slides in a circular disc (radius 100 mm) which moves on three balls around a centering tap. On the vertical edge of the rotating disc a graduation from 0° to 360° was machined in order to permit a direct observation of the angle $\theta$. This was made possible by illuminating the pointer and the scale and by using a magnifying tube, looking through a rectangular lucite window which was arranged in the spectrometer wall for that purpose. Because of the large circumference of the disc the graduation could be accurately read and reproduced to within 0.2°. The centering with respect to the converter was such that $a$ could be held constant to within 0.3 mm. The resulting error is small enough to escape detection, i.e. no systematic difference could be detected between photolines recorded for $\theta$-values, symmetric with respect to the spectrometer optical axis ($\theta = 0$). By setting the screws of the "lower basement" (Fig. 3) the horizontality of the plane of the source movement could be adjusted to within 0.3%. The "upper basement", on which the disc turns, can be moved along the spectrometer axis and the whole arrangement can be adjusted in the direction of the spectrometer radius.

The size of the spectrometer vacuum chamber permits arranging a fairly effective shielding between the source and the detector. Also, aluminium-lined lead bricks were put in on the source side of the baffle in order to attenuate the direct irradiation of the spectrometer walls around the electron beam. For detection we used a plastic scintillator equipment (Stockendal and Hultberg, 1959).

The source-converter distance was chosen to be $a = 30$ mm. After a careful adjustment of the motion of the gamma-ray source around the converter centre, line spectra of the $K$, $L$ and $M'$ photoelectrons were recorded for each of a

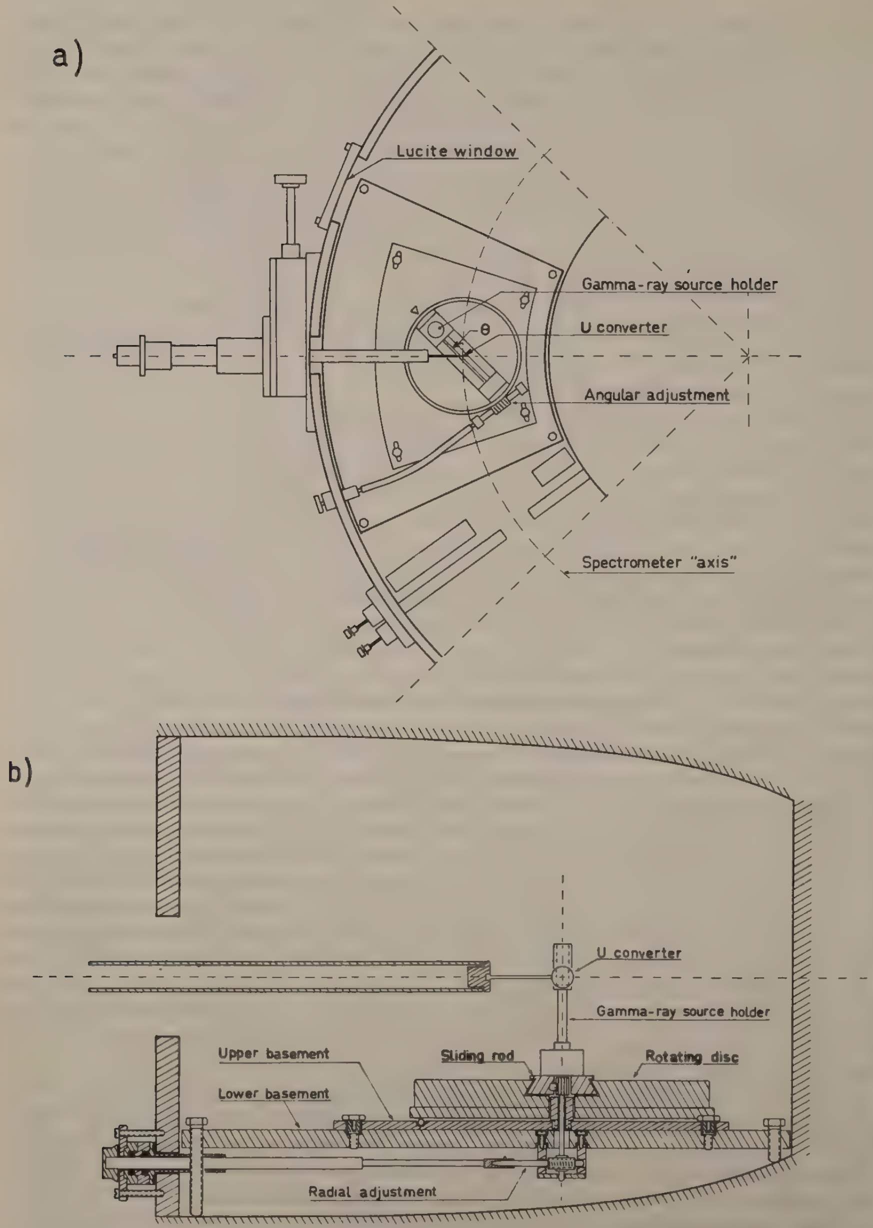

Fig. 3. Mechanical construction, used with the double-focusing spectrometer, for the study of the photoelectric angular distributions. The quantities $\theta$ and $a$ (Fig. 2) can be adjusted from outside the spectrometer.

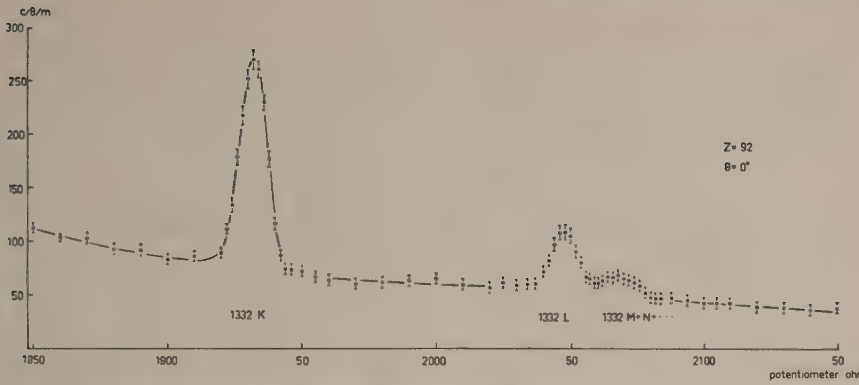

Fig. 4. Photoline spectrum for a specific value of $\theta$, as recorded in the double-focusing spectrometer. $h\nu = 1332$ keV. A 2.2 mg/cm$^2$ U converter with 7.3 mm radius was used. The resolution is 0.7 %.

number of different settings of $\theta$. For a specific angle, Fig. 4 illustrates the measurements at one of the gamma-ray energies. Apart from the intensity variation the spectra were similar in all cases, except for a slight change in resolution with energy. From Fig. 4 it is seen that the instrumental resolution (0.7%) did not allow either a separation of the $L$ subshells or of the $M$, $N$, . . . shells. The continuum was carefully recorded in order to allow a satisfactory interpolation of the background under the peaks. For the purpose of checking such interpolations the continuum was measured, in some cases, with the converter replaced by an aluminium disc. No significant error in the interpolation procedure could be detected, due to the general smoothness of the continuum. Complete spectra (as shown in Fig. 4) were recorded for a number of angles, at each of the three energies. By plotting the photoline areas versus $\theta$, experimental representations $J_e(\theta)$ were obtained for the angular functions, per unit solid angle (Fig. 5), with help of the fitting of polynomials of degrees 8–10 according to the method of least squares. The calculations were carried out on the electronic computor BESK.

The errors in the determination of the photoline areas vary strongly with $\theta$ for each distribution. Individual estimates are given in Fig. 5. The latter are in agreement with check recordings and with earlier experiments performed by the author.

The normal through the converter centre defines the direction $\theta = 0$ which here is tangent to the spectrometer axis. The graduation of the rotating disc had an arbitrary orientation and, consequently, had to be normalized by a determination of the angle, corresponding to $\theta = 0$. Because the angular distributions are symmetric in half-planes, separated by the directions $\theta = 0$ and $\pi$, the $\theta = 0$ direction can be inferred from the symmetry of a "double" distribution (recorded from 0° to 360°). Such measurements were carried out for the $K$-shell distributions at each of the three energies (Hultberg and Novakov, 1957). The results for the normalization agreed to within 0.5° and, also, with a purely geometrical determination. Moreover, the constancy of the normalization was tested and found satisfactory for different radial distances $a$.

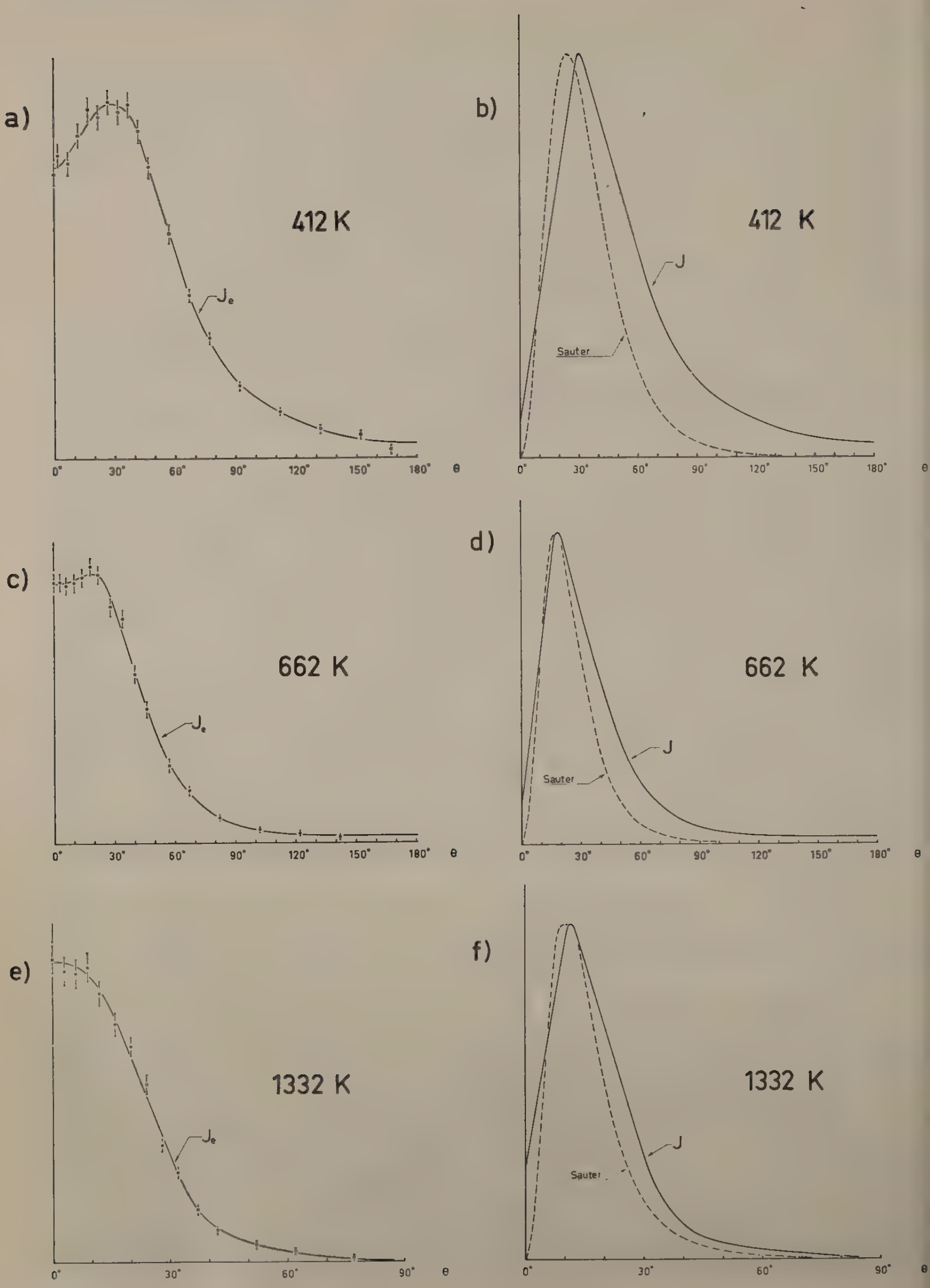
a)
412 K
$J_e$
0° 30° 60° 90° 120° 150° 180° θ
b)
412 K
J
Sauter
0° 30° 60° 90° 120° 150° 180° θ
c)
662 K
$J_e$
0° 30° 60° 90° 120° 150° 180° θ
d)
662 K
J
Sauter
0° 30° 60° 90° 120° 150° 180° θ
e)
1332 K
$J_e$
0° 30° 60° 90° θ
f)
1332 K
J
Sauter
0° 30° 60° 90° θ

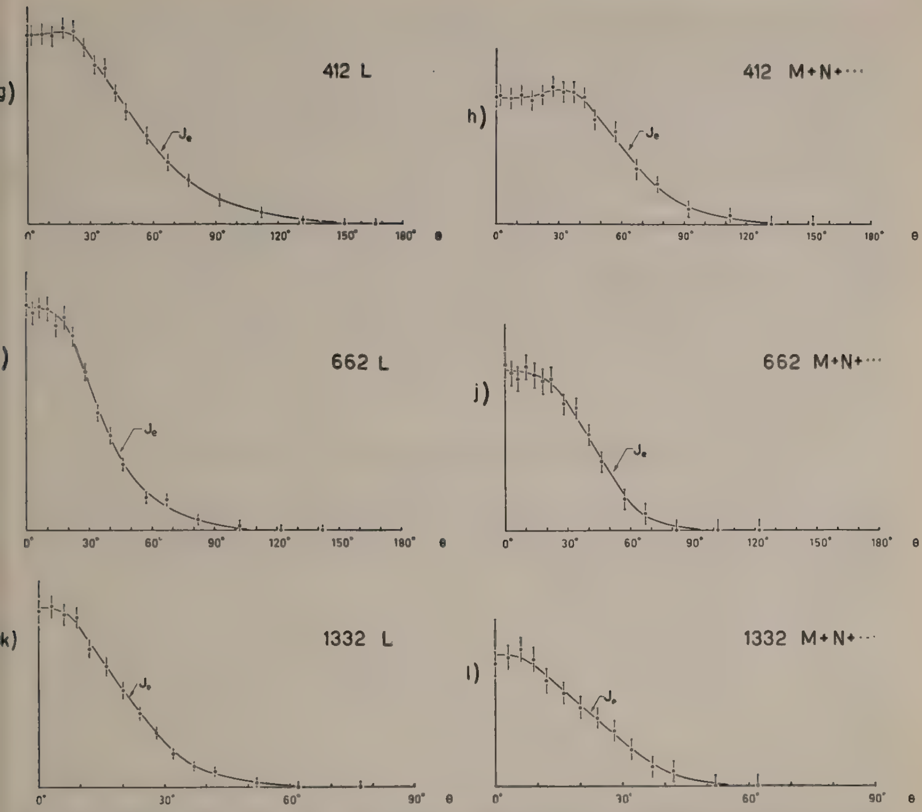

Fig. 5. Representations of the longitudinal angular dependence of the photoelectric effect, per unit solid angle, for the $K$, $L$, and $M+N+\cdots$ shells. Estimated experimental uncertainties are indicated. The curves marked $J_e$ contain distortions, due to geometry and scattering ($\theta_0 = 14°$, $d = 2.19$ mg/cm$^2$, cf. p. 329). The notation $J$ means that the corresponding functions should represent "true" angular distributions. The comparison with Sauter is made on the basis of his approximate expression (22). Energies are in keV.

A few remarks should be made regarding the phenomenon of backscattering against the material supporting the uranium, because a possible effect of this kind would tend to increase the observed intensities to an extent, which depends upon $\theta$. On account of the character of the distributions such an influence would introduce serious errors only at very high angles, where the intensities become low. For the following reasons we do not, however, believe that, as a consequence of large-angle scattering, the curves of Fig. 5 would be caused to fall outside the error limits indicated. In the first place, no appreciable angular variation of the photoline widths was observed, indicating that a possible backscattering effect would necessarily have to be produced by elastically scattered electrons (single scattering). The probability for single scattering is, however, small compared with that of ordinary multiple scattering, as can be seen from the theory of Molière (1948), where the transition from multiple scattering to large-angle single scattering is obtained. Moreover, by comparison with earlier recordings, where the uranium was put on a thinner Al backing, no deviation outside the indicated errors was observed. Also, it should be noticed that while the intensities of the $L$ and $M'$ distributions at 412 keV are not observable above $\theta = 150^\circ$ and $140^\circ$, respectively, the $K$ distribution at 662 keV is measurable at these angles. Since the scattering probability increases when the energy decreases, it seems probable that here the actual amount of backscattering must be small. Consequently, we believe that the backscattering effect will not significantly alter the shape of the curves of Fig. 5. It may also be remarked that, in the application of the angular distributions to the determination of gamma-ray intensities (see section H), the ordinates at angles $\theta > \pi/2$ enter only in products with $\sin\theta$ which means that the uncertainties at large angles are diminished (cf. Fig. 13).

## E. The experimental distribution function and its properties

In the preceding section it was described how we arrived at a certain set of uncorrected angular functions which will be denoted by $J_e(\theta)$. We shall now discuss their properties in order to see how they compare with theory and to investigate their general usefulness.

### *General discussion of distorting effects*

A few preliminary remarks of qualitative character will serve the purpose of fixing the ideas. Because of the finite solid angles that are subtended by (*a*) the converter at the source, (*b*) the baffle at a point on the converter and (*c*) the source at a point on the converter (cf. Fig. 2), it is clear that the uncorrected $J_e$ does not represent the "true" function $J$. Moreover, the thickness of the converter material is finite, i.e. the influence on $J$ from multiple scattering of the electrons in the converter cannot be neglected. In order to be able to make a detailed comparison with theory it will thus be necessary to find methods, effectuating the transition from finite to zero order in the disturbing effects. In the following the latter will often be termed the *geometrical* and the *scattering distortions*, respectively. Qualitatively, $J_e$ results from averaging processes over $J$ with regard to the finite set-up geometry and the scattering. Because the solid angle subtended by the converter at the source strongly depends on $\theta$ (Fig. 2) it is seen that the effect due to the extension of the converter (which constitutes the largest component of the geometrical distortion) is very large at $\theta = 0$ and $\pi$, but is vanishingly small around $\theta = \pi/2$. The multiple scattering, on the other hand, is determined by the directions of the electron paths in the converter material and is independent of $\theta$.

We shall now proceed to the analysis of the geometrical distortion. The multiple scattering which was considered in a very approximate way by Hultberg 1955 will, however, not be analyzed here because a rigorous treatment of this effect is very difficult. The complications arise from the fact that the photoelectrons are emitted in all possible directions from each point of the converter volume. With every such direction is associated an individual material thickness for the particle to traverse. The theories for the treatment of electron scattering always assume a collimated electron beam, traversing a certain thickness of matter, i.e. the initial conditions are the same for all electrons. For every emission direction of the photoelectrons we should then have to consider a large number of very thin layers, perpendicular to the direction in question. The resulting integral equation will be very complicated. Since the angular distribution function has no meaning outside the region $0 \leqslant \theta \leqslant \pi$, the integral equation cannot be of the folding type, because then the integral must extend to infinity. Fortunately, it turns out that the multiple scattering is of importance only at very small angles $\theta$. This was proved from a series of special measurements (see below) wich enabled us to study both distorting effects experimentally. Thus we feel justified in neglecting to perform the very complicated analysis of the multiple scattering which alone would here constitute a qualified scientific problem.

### *Analysis of the angular distribution measurements*[1]

The quantities used below refer to Fig. 2. The radiation source, situated at $Q$, radiates $I_\gamma$ quanta per disintegration and unit solid angle and its strength is $k_\gamma$ disintegrations per second. The absorption of quanta, contained in the solid angle subtended at $Q$ by the surface element $dS$ at $R$ on the converter, is proportional to the beam intensity at $R$ (varying as $1/r^2$) and to the number $dS\,d$ of absorption centra encountered. By multiplication with the probability per unit solid angle $N\,J(\vartheta+\Delta)$ that a photoelectron be emitted in the direction $\vartheta+\Delta$ and by introduction of the solid angle $\Omega_e$, subtended by the aperture at $R$, we obtain, after an integration over the converter, the total number of photoelectrons through the aperture as (cf. Hultberg and Stockendal, 1959 *a*)[2]

$$A_\gamma(\theta) = I_\gamma k_\gamma d\,b\,N\,\Omega_e \int_C J(\vartheta+\Delta)\frac{dS}{r^2} = K\,\Omega_e \int_C J(\vartheta+\Delta)\frac{dS}{r^2} \tag{30}$$

with

$$K = I_\gamma k_\gamma d\,b\,N. \tag{30$'$}$$

$b$ is a dimension factor (Hultberg and Stockendal 1959 *a*), $N$ was defined in section B. The angle $\theta$, defining the source position, is a constant during the integration, implying that $A_\gamma$ be a function of $\theta$, as indicated. Eq. (30) is strictly valid only for a converter sufficiently thin for the multiple scattering to be disregarded. The transition to the more practical case of a finite converter thickness can be made in a formal way by writing

$$J'(\theta) = \mathrm{op}\,J(\theta), \tag{31}$$

where "op" denotes an operator for which no explicit expression will be given here (cf. discussion above). It merely serves to indicate the kind of influence exerted on $J$ by the action of the scattering; the effect is that of redistributing the function $J$, with $J'$ as a result, under the restriction that

$$\int_0^\pi J'(\theta)\,\sin\theta\,d\theta = \int_0^\pi J(\theta)\,\sin\theta\,d\theta, \tag{32}$$

---

[1] This sub-section was worked out in cooperation with H. Rådström, Division of Mathematics, The Royal Institute of Technology, Stockholm 70.

[2] The finite size of the source and the aperture will introduce negligible distorsions (see below).

implying that the *total* number of photoelectrons, emitted from the converter, cannot be changed by an angular redistribution of the emitted intensities. Such a condition must hold as long as no photoelectrons are absorbed in the converter material. Generally, it is not difficult to satisfy the latter requirement in practice. We shall then write for the angular function per unit solid angle, as obtained in the measurements of section D,

$$J_e(\theta) = A'_\gamma(\theta) \,/\, \Omega_e = K \int_C J'(\vartheta + \Delta)\, dS \,/\, r^2. \tag{33}$$

With a satisfactory approximation it is assumed that the order of the signs "op" and $\int_C$ can be reversed. There are experimental indications that such an assumption is reasonable (cf. the extrapolation measurements below), implying that the processes may be treated independently of each other. In (33) we introduced the previously used notation $J_e$ for the *experimental* distribution function. Changing $\Omega_e$ to the spectrometer transmission constant $c_\gamma$, Eq. (33) will represent the angular measurements, as presented in Fig. 5.

In order to obtain a useful form of Eq. (33) we shall consider the curves, in the converter plane, along which $J'(\vartheta + \Delta)$ or, to a sufficient approximation, $J'(\vartheta)$ is constant. The niveau curves will be circular arcs with $T$ as centre (Fig. 2). For element of area $dS$ we then take $dS = s\,dx$, where $s$ denotes the part of the circular arc lying inside the converter area, represented as a circular disc of radius $c$. When $\theta = 0$, $T$ coincides with the converter centre $O$ and we have $s = 2\pi x$, i.e. $s$ forms concentric circles. The latter is the case discussed by Hultberg and Stockendal 1959 *a*. When $\theta$ increases $T$ moves away from $O$ and $s$ partly forms concentric circles and partly circular arcs, and when $a \sin\theta > c$, $s$ only forms circular arcs. The quantities $r$, $\vartheta$ and $\Delta$ are given by

$$\left.\begin{aligned} &\vartheta = \operatorname{arc\,tg} \frac{y}{a\cos\theta} \\ &\Delta = x/m, \\ &r^2 = (a\cos\theta)^2 + (a\sin\theta + x)^2. \end{aligned}\right\} \tag{34}$$

Eq. (33) can then be written

$$J_e(\theta) = K \int_{-c}^{+c} J'(\theta, x)\, \frac{s(\theta, x)}{r^2}\, dx, \tag{35}$$

where the independent variable $x$ is introduced [$\vartheta = \vartheta(\theta, x)$ and $\Delta = \Delta(x)$].

(35) can be recognized as an integral equation from which we are interested to determine the unknown function $KJ'$. The function $s(\theta, x)/r^2$ is called the *kernel* of the integral equation. In an integral equation the unknown function is usually written as depending on only one variable and the integral can easily be transformed so as to conform with current notation practice. However, for the numerical treatment the form of Eq. (35) has turned out to be more convenient.

The solution of Eq. (35) belongs to a class of problems, encountered in experimental physics, where it is necessary to remove disturbing effects which originally had to be introduced in order that it be possible to perform the desired investigation. A special case is that of the so-called folding or convolution integral which was applied to the present problem by Hedgran and Hultberg (1954) and

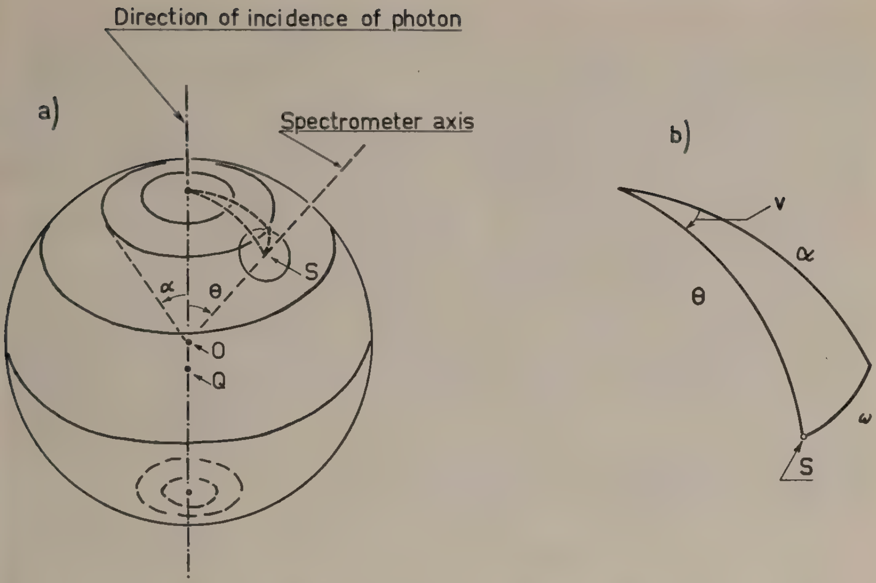

Fig. 6. (*a*) A perspective diagram, showing the photoelectric emission from the point $O$ as niveau lines on a unit sphere. The gamma-ray source is at $Q$. The direction $QO$ is here regarded as fixed in space, and it is imagined that the aperture (with centre $S$) moves around $O$ on the sphere. A particular aperture position is shown. (*b*) The spherical triangle, indicated in (*a*), is shown enlarged.

by Hultberg (1955), as the simplest possible approximation. Their results are, however, not quite reliable because the distributions were not measured for all angles and because the correct expression (35) is not of the folding type. Unfortunately, it seems that no great attention has been paid, in the literature, to the solution of equations similar to (35) for the case where the left-hand side represents physical measurements with intrinsic uncertainties.

In order to solve Eq. (35) for $KJ'$ an iteration method was tried, using the Swedish fast electronic computor BESK. It would have been completely impossible to carry out the calculations without the help of such a machine. As the first approximation $f_1$ we simply use our measured function $J_e$ and obtain the first integral $h_1$ (the integration limits and a constant are omitted, for simplicity):

$$h_1 = \int J_e\, s\, dx/r^2 = \int f_1\, s\, dx/r^2.$$

$h_1$ is then compared with $f_1 = J_e$, towards which the successive iteration integrals $h_i$ must converge. A better approximation $f_2$ is then found by putting

$$f_2 = f_1 - \lambda\,(h_1 - f_1)$$

or, more generally,

$$f_{i+1} = f_i - \lambda\,(h_i - f_1), \tag{36}$$

where

$$h_i = \int f_i\, s\, dx/r^2.$$

The method converges when lim $h_i = f_1$ as $i$ becomes large, in which case $f_{i+1} = f_i$. It should be noted that, in general, not all $\lambda$-values make the process convergent. We tried $\lambda = 1$, for simplicity. It was found that the process was convergent at all points, except in the vicinity of $\theta = 0$ and $\theta = \theta_m$. By help of extrapolation to $\theta = 0$ and interpolation in a small region around $\theta_m$ it was, however, possible to arrive at an acceptable solution after carrying out some 6–8 iterations. Because the integral $h$ of the accepted solution was well inside the experimental errors for all angles it was concluded that the solution obtained was reasonable.

The spectrometer aperture can be regarded as approximately circular. Its role in the present measurements can be studied with help of Fig. 6.

Fig. 6 gives a schematic illustration of the photoelectric emission through the aperture, when the point of emission is situated at $O$. For simplicity, we regard the direction $QO$ as fixed in space and let the aperture move around $O$ on the sphere with the converter-aperture distance $m$ as radius. The total photoelectric intensity, radiated in the differential cone $(\alpha, \alpha + d\alpha)$ around the direction $QO$, is $2\pi J'(\alpha) \sin\alpha \, d\alpha$, where the use of the notation $J'$ serves to indicate that here the photoelectric function to be introduced may already contain some kind of deformation. Obviously, only the proportion $v/\pi$ can get through the aperture. Solving the spherical triangle of Fig. 6*b*, we obtain

$$\begin{aligned} J''(\theta) &= \frac{1}{2\pi(1-\cos\omega)} \int_0^\pi \frac{v}{\pi} 2\pi J'(\alpha) \sin\alpha \, d\alpha \\ &= \frac{1}{\pi(1-\cos\omega)} \int_0^\pi v J'(\alpha) \sin\alpha \, d\alpha \end{aligned} \tag{37}$$

where
$$v = \arccos \frac{\cos\omega - \cos\theta \cos\alpha}{\sin\theta \sin\alpha}$$

It is understood that $v = \pi$ if $\cos v \leqslant -1$ and $v = 0$ if $\cos v \geqslant 1$. In the present measurements $\omega \sim 5^\circ$. On the unit sphere, $2\pi(1-\cos\omega)$ is the area of the aperture, over which the integral is to be taken. Outside the aperture, $v$ is defined as zero.

We can now study the effect of the spectrometer aperture by taking one of the distributions of Fig. 5 and evaluating $J''(\theta)$, according to Eq. (37), for different dimensions of the aperture. The result is $J''(\theta) = \text{const}\ J'(\theta)$, at all angles $\theta$, provided the aperture extension is not too large. The latter condition is fulfilled to a sufficient approximation when the diameter of the aperture is seen from a point on the converter under an angle of $2\omega < 15^\circ$. In our case $2\omega$ is about $10^\circ$. We therefore conclude that the finite dimensions of the spectrometer aperture do not disturb our measurements (this was also confirmed by direct experiments). The aperture can thus be represented by a constant $\Omega_e$, as was done in Eq. (30).

The ratio between the angles, under which the converter is seen from the gamma-ray source and the source from a point on the converter, was about 8 in our measurements. Because the width of the total "window" curve approximately results from a quadratical addition of the component widths, the ratio between the distorting effects from the converter and the source dimensions should be about 64. Thus, we can neglect the source size and, consequently, Eq. (30) correctly describes the photoelectric intensity through the aperture if $J'$ is substituted for $J$.

*Extrapolation measurements*

In the preceding part of the present section we have discussed the processes underlying the experimental results, reported in section D. The important consequences were the insight into the mechanism of the action of the experimental set-up and the possibility of representing the experimental results by Eq. (35). It was also reported that the latter expression had been the object of some numerical work, in order to "reduce" the disturbing effect of the converter geometry to zero. However, some limitations are apparent. In the first place, solving Eq. (35) does not yield the final result, since the solution $J'$ still contains a distorsion, due to scattering. As mentioned above, we have not tried to find the formal relation between $J'$ and $J$. Secondly, it has not been possible to prove, in a mathematically rigorous way, the full reliability of the iterative method of solving Eq. (35), or of its uniqueness.[1] Thus, for several reasons it was felt that an *experimental* effort towards the complete solution of Eq. (35) should be of great value. It was also hoped that, as a partial result, it would be possible to test the numerical treatment of the converter geometry.

The obvious procedure to follow would be to repeat the angular measurements at higher resolutions with respect to geometry and scattering. In practice, this meant recording the angular distributions, using larger source–converter distances $a$ and thinner converters. In order to characterize the "resolution" used, we will define the *geometrical resolution* by specifying an angle $\vartheta_0$ (in degrees) such that the converter radius is seen under the angle $\vartheta_0$ from the source, when the latter has the position $\theta = 0$. The *scattering resolution* can be characterized by giving the thickness $d$ of the converter.

Since there were reasons to believe that ($a$) the numerical treatment of the converter geometry was reliable at angles $\theta > \theta_m$, and (b) the effect of multiple scattering would be small at $\theta > \theta_m$, it was found suitable to start by testing the validity of these assumptions, as they might prove useful. Thus, at the 662 and 1332 keV energy, additional complete distributions were recorded for the $K$-shell. By comparison of the normalized curves it was found that the assumptions a) and b) were verified within the experimental errors. Thus, when solving (35) at large angles the distortion due to scattering might be neglected, and here our numerical method will approximate the true distribution. Moreover, it should be observed that the condition (32) is approximately valid also for the geometrical distortion. Thus for any of our $J_e$, we have

$$\int_0^\pi J_e(\theta)\sin\theta\, d\theta = K\int_0^\pi J(\theta)\sin\theta\, d\theta, \tag{38}$$

where $K\,J(\theta)$ represents the true distribution, as it will be inferred from our experiments. Neglecting absorption processes, Eq. (38) simply expresses the fundamental fact that an emitted electron must be detected *somewhere* in space. If, in addition, the ratios at infinite resolution

$$\varkappa_0 = J(0)/J(\theta_m), \qquad \varkappa_\pi = J(\pi)/J(\theta_m) \tag{39}$$

---

[1] Recently, H. Rådström and J. Philip used another method for the numerical solution of Eq. (35). They have proved that their method converges. It is a variational method, where a certain sum of squared errors is minimized. Their numerical results confirm the results of our calculations, described above (private communication).

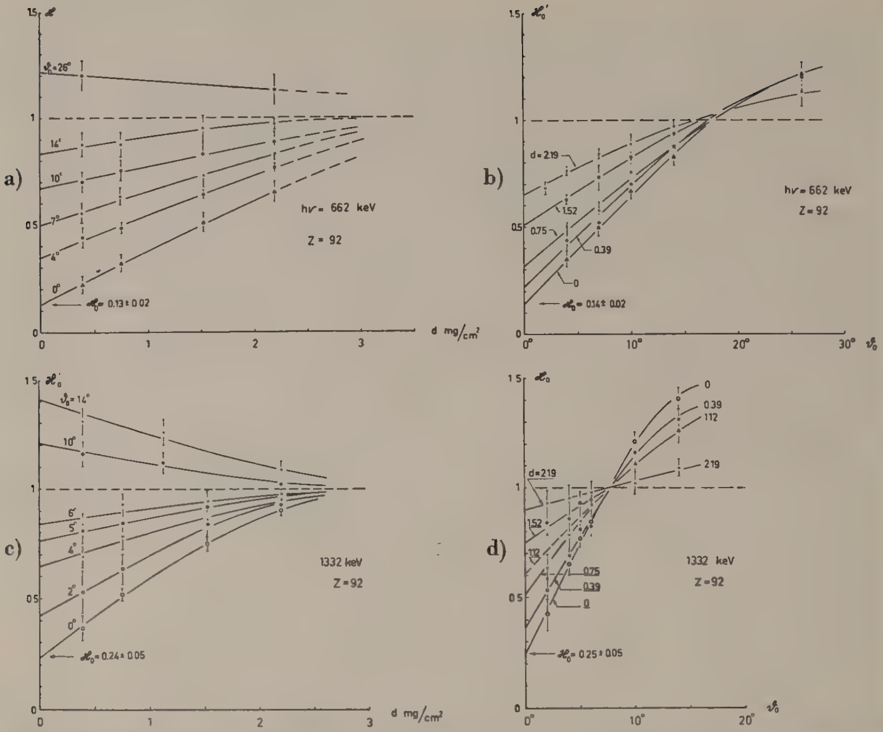

Fig. 7. Experimental determinations of the ratio $\varkappa_0' = J_e(0)/J_e(\theta_m)$ for the $K$-shell, at two gamma-ray energies. $\varkappa_0'$ is plotted as function of both $d$ and $\vartheta_0$. By extrapolation to $\vartheta_0 = 0$ and $d = 0$ the ratio at infinite resolution, $\varkappa_0$, can be found. $\vartheta_0$ and $d$ can be reduced in any order.

were known, we might be able to construct reasonable representations of $KJ$, using (38), (39) and, at large angles, the above-mentioned calculations. Since the $J_e$ functions are practically constant over a large angular interval around $\theta = \pi$, no distortions will be introduced here by the experiments. Thus, in order to obtain $\varkappa_0$ and $\varkappa_\pi$, it is only necessary to measure $\varkappa_0'$ (the prime indicates that the resolution is finite) by recording $J_e(0)$ and $J_e(\theta_m)$, at a number of different resolutions, and try to extrapolate the results to $\vartheta_0 = 0$ and $d = 0$. Such experiments were recently carried out for the $K$-shell. The results are illustrated in the diagrams of Fig. 7, where $\varkappa_0'$ is given as function of both $\vartheta_0$ and $d$. The estimated errors in the photoline ratios are indicated.

It is interesting to observe that, at small $\vartheta_0$ and $d$, the only reasonable curves to fit to the experimental points are straight lines. Extrapolating the latter in the $\vartheta_0$ diagram to zero gives the $\varkappa_0'$ ratios for infinite geometrical resolution. Inserting the latter ratios into the $d$-diagram and extrapolating to zero, a second time, gives the desired $\varkappa_0$, at the respective energy. It is gratifying to observe that $\varkappa_0$ remains unchanged if the procedure is carried out in the reverse order, i.e. first reducing $d$ to zero and then $\vartheta_0$. This may be taken as an indication

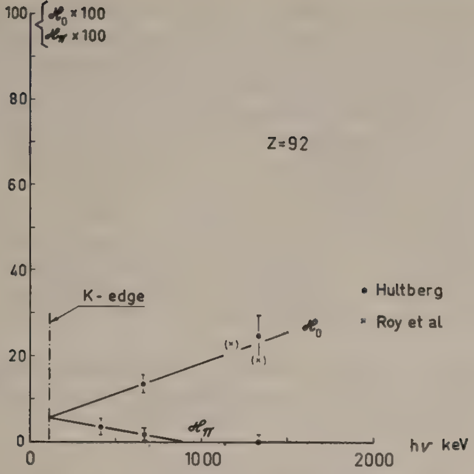

Fig. 8. The $K$-shell ratios $\varkappa_0$ and $\varkappa_\pi$ as functions of the gamma-ray energy. The converter material is uranium. The crosses were obtained from a diagram by Roy *et al.* (1955). These authors do not, however, give any indications about their experimental errors, and it is impossible to estimate the latter from their diagram, which is of a very inferior quality. Nevertheless, some regard was paid to the crosses in drawing the $\varkappa_0$ curve.

that the geometrical and scattering distortions take place independently of each other. It will, consequently, be possible to obtain, from Fig. 7, $\varkappa_0'$ ratios valid for a certain amount of multiple scattering, but free from any geometric distortion. The latter ratios can then be used to check the results of the computational method for the reduction of $\vartheta_0$. When carrying out such a comparison it was seen that the computations gave reasonable results, although there was a slight tendency in the calculations to give low $\varkappa_0'$ ratios.

From the $d$-diagrams of Fig. 7 it seems probable that $\varkappa_0' = 1$ is an asymptotic limit, and from the $\vartheta_0$ diagrams that $\varkappa_0'$ takes the constant value 1 at a particular $\vartheta_0$ value, independently of $d$. These features are consistent with the observations that an increase in $d$ tends to smooth out the photoelectric anisotropy, and that an already isotropic distribution will remain undisturbed by scattering.

Using (*a*) the iterative calculations, (*b*) the experimentally corroborated observation that the electron scattering has a negligible influence, as long as the derivative of the distribution does not change too abruptly, (*c*) the found $\varkappa_0$ ratios, and (*d*) the condition (38), it was finally possible to construct curves, at $h\nu = 662$ and 1332 keV, which should represent the true photoelectric longitudinal distributions, apart from a factor $K$. From the latter functions we can then obtain the respective $\varkappa_\pi$ ratios.

At the 412 keV energy, where no extrapolation measurements were carried out, the geometric distortion is small. A comparison with earlier measurements at this energy shows that also the scattering distortion is sufficiently small to be neglected at $\theta > \theta_m$. From the $\varkappa_0$ values of the two higher energies it seems reasonable that, at 412 keV, $\varkappa_0$ takes a value somewhere in the region 0.07–0.12 (cf. Fig. 8). From the construction of a preliminary $KJ$ function we could then obtain a $\varkappa_\pi$, largely insensitive to the exact value of $\varkappa_0$. Fig. 8 gives a diagram of $\varkappa_0$ and $\varkappa_\pi$ versus the gamma-ray energy. Although the errors in $\varkappa_\pi$ necessarily are quite large it is seen that the points are consistent with the reasonable assumption that $\varkappa_0 = \varkappa_\pi$ at the $K$-edge, where the longitudinal angular distribution should be symmetric about $\theta = \pi/2$. With help of the latter assumption we obtain the full-drawn curves of Fig. 8, enabling us to construct the true distribution at $h\nu = 412$ keV.

From Fig. 8 we obtain:

| $h\nu$ | 116 | 412 | 662 | 1332 |
|---|---|---|---|---|
| $\varkappa_0$ | $0.06 \pm 0.03$ | $0.10 \pm 0.02$ | $0.135 \pm 0.02$ | $0.245 \pm 0.05$ |
| $\varkappa_\pi$ | $0.06 \pm 0.03$ | $0.035 \pm 0.02$ | $0.02 \pm 0.015$ | 0 |

The true photoelectric $\theta$-distributions for the $K$-shell, thus inferred from our experiments, are shown in Fig. 5 *b*, *d*, *f*. Table 2 of section H gives numerical values for the ordinates versus $\theta$.

## F. Theory and experiment

As results of the present investigations we have introduced certain corrected experimental functions which should represent true photoelectric $\theta$-distributions, per unit solid angle, apart from an arbitrary factor. In the case of the uranium $K$-shell these functions are compared, in Fig. 5, with Sauter's formula (22). For the $L$ and $M + N + \cdots$ shells, however, only the uncorrected experimental functions are given, since here no extrapolation measurements were carried out. Also, the theoretical difficulties, which are large already for the $K$-shell, increase rapidly with higher shells (no relativistically correct expressions have been given), complicating the comparison with experiment. We shall, therefore, content ourselves with a discussion of the $K$-shell distributions.

In section B some quantities were quoted, upon which a comparison between theory and experiment could be based. Before going into details it should be pointed out that it is not yet possible to carry out a really satisfactory comparison because no theoretical data, valid for $Z = 92$, have been presented. Thus, from a comparison of our experiments with formula (22) we cannot judge the underlying theory as such, but only tell how good is the approximation (22).

### *The shape of the distribution function*

Expression (22) was obtained under the restriction that

$$Z \ll 137. \tag{40}$$

This means, physically, that binding energies are neglected, as can be seen from the fact that (22) depends only on the velocity parameter $\beta$ of the photoelectron. For $Z = 92$ the condition (40) is not valid and we may expect to find deviations from (22). From Fig. 5 it is seen that the experimental intensities are larger, particularly at $\theta = 0$ and $\pi$, and that the experimental values of the angle of maximum emission $\theta_m$ are slightly larger.[1] The existence of a finite photoelectric emission in the direction $\theta=0$ was first pointed out by Hedgran and Hultberg (1954) and Hultberg (1955). This observation was theoretically confirmed by Sauter and Wüster (1955) who removed the limitation (40) by carrying out numerical calculations from exact expressions. They obtained $\varkappa_0=0.27$ at $h\nu=1332$ keV, in satisfactory agreement with our result $\varkappa_0=0.245$ (section E). Cloud chamber experiments at the gamma-ray energies 1172 and 1332 keV (Roy *et al.*, 1955) also revealed a finite intensity at $\theta=0$ (Fig. 8). From Fig. 1 of the latter paper it is seen that the order of magnitude of the forward intensity at 1332 keV agrees with our value. According to the authors the latter experiments were, however, not reliable at large angles and, therefore, they cannot be further compared with our results. From the present measurements it seems obvious that there can also be a finite photoelectric emission in the *backwards* direction $\theta=\pi$, as can be seen from Fig. 8.

It should perhaps be pointed out that the variation of $\varkappa_0$ with energy (Fig 8.) is at variance with certain theoretical arguments by Banerjee (1958). He obtained a closed expression for the $\theta$-dependence in the limit that $a/k$ is small, where $a=Z/137$ and $k=h\nu/mc^2$. However, his expression does not extend further than (22), although it represents a higher approximation, since his formula also requires that $J(0)=0$.[2] He accepts $\varkappa_0=0.27$ at 1332 keV but argues that $\varkappa_0$ should decrease as the gamma-ray energy increases, on the basis of his formula which should be true at extreme energies, where $a/k$ becomes small. However, nothing is stated about $\varkappa_\pi$. We do not understand this discrepancy because our experiments clearly indicate the reverse variation in $\varkappa_0$. Because of the satisfactory agreement for our $\varkappa_0$ with Sauter's theory, so far, an agreement with Banerjee's reasoning would seem to require that $(\varkappa_0)_{662}>(\varkappa_0)_{1332}=0.27$ (see, however, below). As can be understood from Figs. 7 and 8, this is, however, completely outside the experimental error. On the other hand, the character of our results for $\varkappa_\pi$ agree with Banerjee's arguments. Admitting that the simple functional dependence, attempted in Fig. 8, is not strictly true our results might nevertheless be regarded as being consistent with having $\varkappa_0=\varkappa_\pi$ at the $K$-edge, where the $\theta$-distribution should be symmetric about $\theta=90^\circ$ (implying the previous equality). A possibility of reconciling our experiments and the opinions of Banerjee would seem to be the assumption of a maximum in the $\varkappa_0$ curve at medium energies (of the order of a few MeV). We would, however, believe that an asymptotic behaviour is more likely although, at present, such a belief must be largely intuitive. Probably the only way of solving this question is the performance of exact numerical calculations.

A few remarks might be added concerning the obtained $L$ and $M+N+\cdots$ shell functions. From Fig. 5 we can see that the $L$-electrons have a stronger preponderance for emission in the forward directions than the $K$-electrons which is in qualitative agreement with (23). The combined effect of the $M+N+\cdots$ shells seems to be such that the distributions more resemble those of the $K$-shell, except that the intensities drop to zero more rapidly.

---

[1] These features of the experimental distributions are in qualitative agreement with calculations by L. Sliv (private communication, 1955). It might also be pointed out that the *relativistic* term $J_r(\theta)$ of Eq. (22) agrees better with the experiments (apart from $\theta=0$ and $\pi$) than does the *complete* function $J=J_n+J_r$.

[2] It should be noted that formula (31) of Banerjee's paper gives $J(\pi)<0$, which is impossible. This error may be due to a misprint.

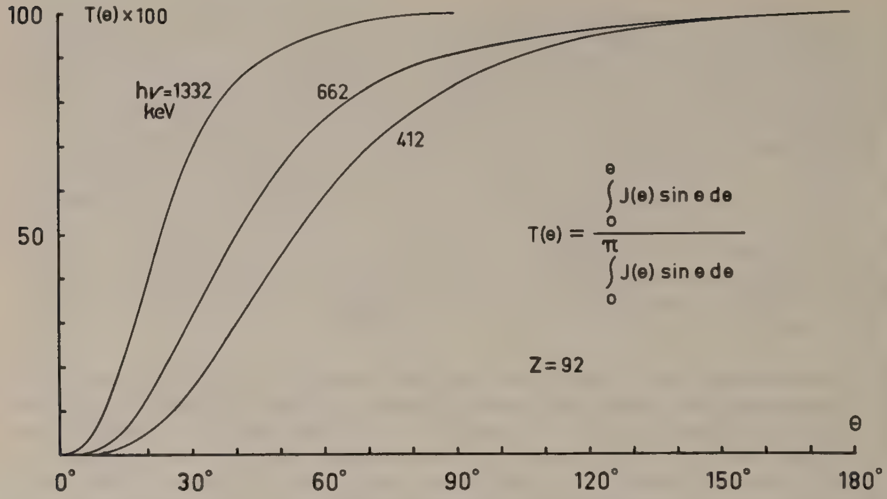

Fig. 9. The function $T(\theta)$ for the uranium $K$-shell as obtained from the data of Table 2.

*Quantities obtained by integration*

In most cases the comparison with theory has been founded on some quantities, obtained by integrating the distributions in different ways (section B). Such a procedure necessarily constitutes a less sensitive method of testing theory than the preceding one. However, due to the poor statistics of the cloud chamber experiments it was difficult to obtain the shape of a particular distribution with an accuracy, sufficient to allow a "differential" comparison.

In section B we defined the quantities $Q$, $\theta_b$ and $R$. The asymmetry ratio $Q$ and the bipartition angle $\theta_b$ are conveniently obtained from plots of $T(\theta)$, defined by (29). Fig. 9 gives $T(\theta)$ for the uranium $K$-shell, as calculated from the data of Table 2. According to formulae (25) and (26), $Q$ and $\theta_b$ are easily obtained from Fig. 9.

From (27) and (28) we can find the ratio $R$ of the average forward momentum of the electron to the total momentum of the incident photon. Using our experimental functions we obtain, for the $K$-shell, the values illustrated in Fig. 10. At the $K$-edge we have $R=0$, corresponding to the situation that the electron is liberated but lacks velocity. At very high energies $\overline{\cos\theta}=1$ and $R=1$.

## G. The relative photoelectric absorption of gamma-rays by the electron shells of the uranium atom. A discussion of the accuracy of available photoelectric cross-sections for $Z=92$

According to Eq. (38) we can write

$$2\pi\int_0^\pi J_e(\theta)\sin\theta\,d\theta=I_\gamma k_\gamma d b\,2\pi N\int_0^\pi J(\theta)\sin\theta\,d\theta$$

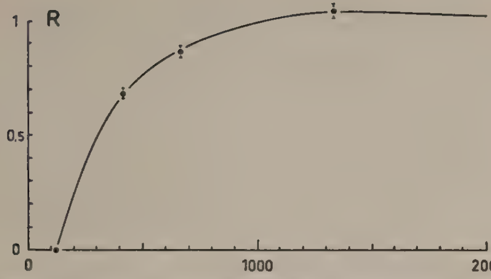

Fig. 10. The ratio $R$ between the average forward momentum of the ejected photoelectron and the total momentum of the incident photon, as function of the gamma-ray energy. $Z=92$.

or, using the definition (24),

$$2\pi\int_0^\pi J_e(\theta)\sin\theta\,d\theta = I_\gamma k_\gamma\,d\,b\,\tau,$$

where $\tau$ is the (total) photoelectric cross-section for a specific shell. In our experiments all parameters were held constant during the measurements of mutually related $K$-, $L$- and $M'$-distributions. Therefore, we can write, for the relative absorption of two atomic shells 1 and 2 (at the same gamma-ray energy),

$$\frac{\tau_1}{\tau_2}=\frac{\left[\int_0^\pi J_e(\theta)\sin\theta\,d\theta\right]_1}{\left[\int_0^\pi J_e(\theta)\sin\theta\,d\theta\right]_2}. \tag{41}$$

Eq. (41) thus permits us to obtain experimental values of the ratios $\tau_K/\tau_L$, $\tau_K/\tau_{M'}$, $\tau_L/\tau_{M'}$ and $\tau_a/\tau_K$, where $\tau_a=\tau_K+\tau_L+\tau_{M'}$. The following values were calculated (cf. Fig. 16):

$$Z=92\begin{cases}\tau_K/\tau_L = 5.3\pm0.2,\\ \tau_K/\tau_{M'}=13.9\pm0.7,\\ \tau_L/\tau_{M'} = 2.6\pm0.15,\\ \tau_a/\tau_K = 1.26\pm0.01.\end{cases} \tag{42}$$

These values were found to be *independent of energy*, within the experimental accuracy. Estimated errors are indicated. From (42) we obtain the absorption ratios of the electron shells of the uranium atom as

$$Z=92\begin{cases}K\text{-shell} & 79.4\pm0.6\ \%,\\ L\text{-shell} & 14.9\pm0.4\ \%,\\ M+N+\cdots\text{ shells} & 5.7\pm0.2\ \%\end{cases} \tag{43}$$

in the energy region covered by our experiments. The ratios (43) do not differ by much from what is expected at the $K$-edge, where extrapolated data are

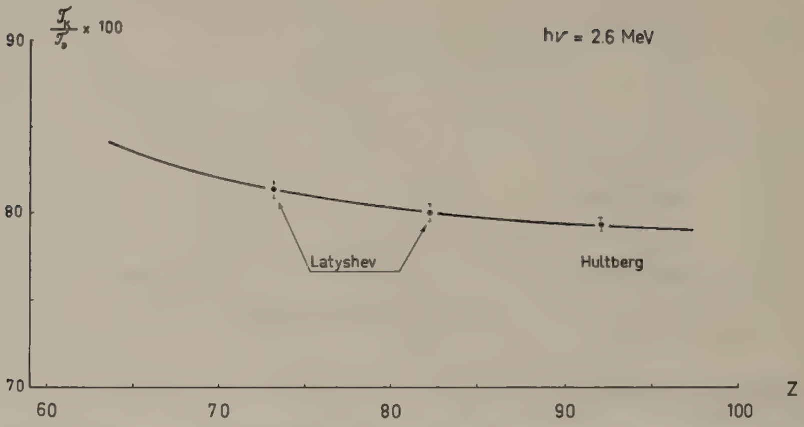

Fig. 11. The contribution of the $K$-shell to the total photoelectric absorption of 2.6 MeV gamma-rays.

available for a large number of elements. The latter information was obtained by extrapolating the results from absorption measurements to the $K$-edge (Kirchner, 1930). Direct measurements of the number of photoelectrons from the different shells have been attempted, using cloud chambers and ionization methods, but the results were not reliable, on account of the poor statistics and of interpretation difficulties. However, the similarity between the $K$-edge values and (43) indicates that the ratios (43) might be valid throughout the beta-spectroscopically interesting region, in agreement with the »5/4 thumb rule», which is sometimes used (Davisson and Evans, 1952), for heavy elements. From studies of photolines, generated in Ta and Pb foils at 2.6 MeV, Latyshev (1947) deduced values for the $K$-shell contribution to the total photoelectric absorption of the gamma-rays, assuming $\tau_L/\tau_M \approx 4$. It should be observed that his values were not obtained from a study of angular distributions and no analysis of converter effects was made. However, because of the high energy the influence from the angular anisotropy is probably small. In Fig. 11 we give Latyshev's and our values for $\tau_K/\tau_a$ versus $Z$. A similar diagram can be found in an article by Grigoryev and Zolotavin (1959), who have compiled absorption ratios (mainly $\tau_K/\tau_L$ values) for various elements, from beta-spectroscopic measurements of photolines. They used a cylindrical converter shape. Assuming the $\tau_L/\tau_M$ ratio to be independent of $Z$ they present, for a number of elements, $\tau_K/\tau_a$ values that are larger than those of Fig. 11 by about 2%. It should be observed that the authors have neglected the influence of the angular anisotropy, and thus their values can be expected to contain systematic errors. The latter may not, however, be appreciable if very large angular intervals are utilized, as seems to be the case with the cylindrical converter, shown in Fig. 1 of the Russian paper. In general, the advantage of using a cylindrical shape seems nevertheless questionable because the photoelectrons have to traverse very different path lengths inside the converter material, leading to a broadening of the photolines and complicating their analysis.

The apparent independence of the absorption ratios (42) of energy in the case

*Table 1.* Comparison between experimental and tabulated $\tau_K$ values for $Z=92$. $\tau_K$ has been obtained from $\tau_a$ by using $\tau_K/\tau_a$, according to (42). The cross-sections are given in barns and the energies in keV.

| $h\nu$ | Author | Type of experiment | $\tau_a$ | $\tau_K$ | Tabulated $\tau_K$ (White) | $\frac{\text{Tabulated } \tau_K}{\text{Experimental } \tau_K}$ |
|---|---|---|---|---|---|---|
| 412 | Colgate | Absorption measurement | $73.2 \pm 0.2$ | 58.1 | 60.0 | 1.03 |
| 662 | | | $24.9 \pm 0.2$ | 19.7 | 20.7 | 1.05 |
| 1332 | | | $5.9 \pm 0.1$ | 4.7 | 5.5 | 1.17 |
| 662 | Titus | Absorption measurement | 23.9 (1) | 19.0 | 20.7 | 1.09 |
| 1172 | Hultberg & Stockendal | Direct observation | | $7.2 \pm 0.5$ | 6.9 | 0.96 |
| 1332 | | | | $5.4 \pm 0.3$ | 5.5 | 1.02 |

(1) Obtained by extrapolating Titus's results.

of $Z=92$ and the similarity of the response of the different elements to the photoelectric effect gives hope that the $\tau_K/\tau_a$ ratios at the $K$-edge may be used quite generally. For the determination of $\tau_a$ it is customary to multiply $\tau_K$ by an estimated $\tau_a/\tau_K$ ratio. Thus, Davisson and Evans (1952) used the 5/4 rule throughout, while White (1957) preferred to approximate $\tau_a/\tau_K$ by theoretical estimates of $\tau_{K+L+M}/\tau_K$. For $Z=92$, the latter ratio was taken as 1.167, below $h\nu=340$ keV, and as 1.138 above that energy. Clearly, the latter factors are too low. At present the best procedure would seem to be using the experimental $\tau_a/\tau_K$ ratios of the $K$-edge throughout the energy region. This method has the obvious advantages of (*a*) taking all atomic shells into account and (*b*) avoiding the use of the very approximate and poorly verified formulae for the $L$- and $M$-shell absorptions.

Using (42) it is now possible, for uranium, to make a direct and accurate comparison of absorption measurements with the theory of the $K$-shell photoeffect. Probably the most accurate experiments of the latter kind are those of Colgate (1952). He gives values for $\tau_a/Z^5$ for different absorbers from which $\tau_a$ can be obtained. Recently, Titus (1958) carried out absorption measurements for three elements of $Z=29$, 47 and 79, at the gamma-ray energy 662 keV. Plotting his $\tau_a$ versus $Z$ in a log-log diagram a straight line can be drawn through the points, making an extrapolation to $Z=92$ fairly safe. Hultberg and Stockendal (1959 *b*) made absolute determinations of $\tau_K$ at 1172 and 1332 keV. In Table 1 we compare the experimental values of $\tau_K$ with White's tables.

It should be remembered that the $\tau_K$ values of the absorption measurements were obtained after subtraction of contributions due to scattering and, above 1.02 MeV, pair production. Thus, the high accuracy claimed by Colgate seems somewhat questionable, particularly at 1332 keV, where the photoelectric effect is small compared with scattering. From the measurements by Hultberg and Stockendal (1959 *b*) it is seen that the accuracy of the tabulated photoelectric cross-sections extends over the critical region at about 1100–1200 keV, where available theories have difficulties. Since the theory of inelastic scattering is considered to be verified to the order of a few percent and since, in this case, the pair production cross-section is small compared with $\tau_K$ we can find no obvious explanation for the discrepancy in $\tau_K$ between Colgate's and our measurements at 1332 keV.

As a result of Table 1 and of an accumulated experience of absolute measurements of interval conversion coefficients (Hultberg and Stockendal, 1959 *a*; Stockendal and Hultberg, 1959) we believe that the photoelectric cross-sections $\tau_K$, as derived from White's tables are good too about 5% in the energy region 300–2000 keV. Since there are no apparent reasons why the accuracy should be substantially less at lower and at higher energies, where it should be easier to find asymptotically correct formulae (of exact validity at either the $K$-edge or at infinity), we feel that the accuracy of the tabulated photoelectric cross-sections might well be the same for all energies.

It was found that the relationship

$$^{10}\log(k^3\tau_K) = 1 + \sqrt{-0.07 + 0.38\,k + 0.005\,k^2}$$

represents White's $K$-shell photoelectric cross-sections to within 10% in the energy region 250 keV $< h\nu <$ 3 MeV. Here $k = h\nu/mc^2$, and $\tau_K$ is obtained in barns. The expression originated from the observation that $k^3\tau_K$ lies very nearly on a parabola for the indicated energy region, if it is plotted logarithmically versus a linear scale in $k$. To obtain better agreement at high energies, a quadratic term in $k$ was added. The expression might be useful for approximate calculations.

With help of (42) it is possible to obtain photoelectric cross-sections for the $L$ and $M + N + \cdots$ shells.

## H. The application of the photoelectric effect to the determination of gamma-ray intensities. The source–converter geometry

In cases of complex decay schemes the beta-spectrometric study of photoelectrons is the only method capable of a resolution high enough to yield detailed information about the intensities of the gamma-rays. It has recently been shown that it is possible to carry out a correct interpretation of photolines, making possible the absolute determination of internal conversion coefficients (Hultberg and Stockendal, 1959), and that the latter technique can be successfully used with complex spectra (Stockendal and Hultberg, 1959). In the present section we shall further discuss the analysis of photolines and treat the generalization of the source–converter geometry to the case of finite dimensions of the gamma-ray source. We shall also give details about our photoelectric angular functions and some directions for their use. Only the case of a flat spectrometer will be treated here although, in principle, the application to the helical type should be equally possible.

Consider the case of a gamma-ray source and a rectangular converter, according to Fig. 12. We always assume a uniform distribution of the converter material.

*The case of a point source*

We obtain from Fig. 12 *a*

$$\left.\begin{aligned} u &= \arccos(h/\varrho), \qquad w = \arccos(c/\varrho),\\ v &= \pi/2 - u - w = \arcsin(c/\varrho) - \arccos(h/\varrho). \end{aligned}\right\} \tag{44}$$

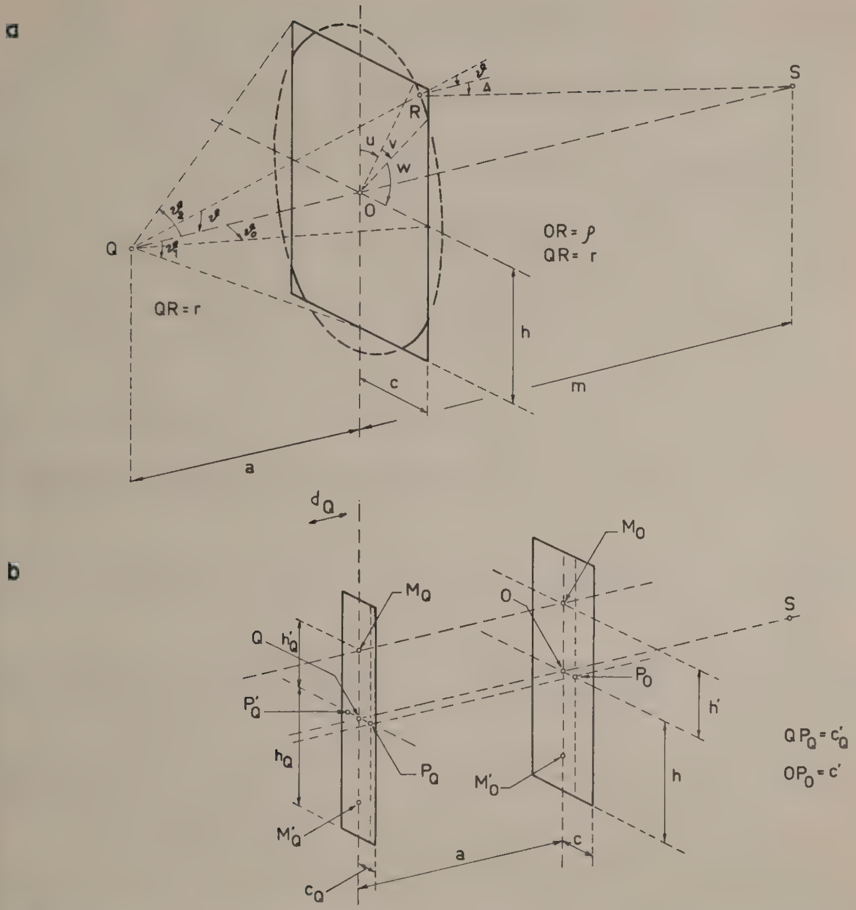

Fig. 12. Schematic illustration of the source-converter geometry. (*a*) A point source is situated at *Q*. On the converter, a "niveau circle" for equal intensity of the incident gamma-rays is shown. The four full-drawn parts of the circle represent the interception by the converter. (*b*) A rectangular gamma-ray source of finite dimensions is centered at *Q*.
It should be noted that Fig. 12 is not drawn to scale.

The surface element $dS$ on the converter surface can then be written $dS = 4\varrho v d\varrho$. Moreover, $\varrho = a \operatorname{tg} \vartheta$, and $r = a / \cos \vartheta$. The photoelectric intensity $A_\gamma$ through the entrance baffle becomes, according to Eq. (30),

$$A_\gamma(\theta = 0) = A_\gamma = K\,\Omega_e \int_0^{\vartheta_2} J(\vartheta + \Delta)\,\frac{4\varrho v\,d\varrho}{r^2}\,.$$

We then obtain for a *rectangular converter*[1]

$$: \qquad A_\gamma = 4\,K\,\Omega_e \int_0^{\vartheta_2} J(\vartheta+\Delta)\,\mathrm{tg}\,\vartheta \left(\mathrm{arc\,sin}\,\frac{\mathrm{tg}\,\vartheta_0}{\mathrm{tg}\,\vartheta} - \mathrm{arc\,cos}\,\frac{\mathrm{tg}\,\vartheta_1}{\mathrm{tg}\,\vartheta}\right) d\vartheta \tag{45}$$

with the supplementary conditions

$$\left.\begin{aligned} \mathrm{arc\,sin}\,\frac{\mathrm{tg}\,\vartheta_0}{\mathrm{tg}\,\vartheta} &= \pi/2, \quad \text{when} \quad \vartheta \leqslant \vartheta_0, \\ \mathrm{arc\,cos}\,\frac{\mathrm{tg}\,\vartheta_1}{\mathrm{tg}\,\vartheta} &= 0, \qquad \text{when} \quad \vartheta \leqslant \vartheta_1, \\ v &= 0, \qquad \text{when} \quad \vartheta \geqslant \vartheta_2, \end{aligned}\right\} \tag{46}$$

and

$$\mathrm{tg}\,\vartheta_0 = c/a, \quad \mathrm{tg}\,\vartheta_1 = h/a, \quad \mathrm{tg}\,\vartheta_2 = \sqrt{h^2+c^2}/a, \quad \mathrm{tg}\,\Delta = (a/m)\,\mathrm{tg}\,\vartheta. \tag{47}$$

If the converter edges are cut along the circle of radius $h$, Eq. (45) simplifies to

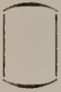

$$: \qquad A_\gamma = 4\,K\,\Omega_e \int_0^{\vartheta_1} J(\vartheta+\Delta)\,\mathrm{tg}\,\vartheta\;\mathrm{arc\,sin}\,\frac{\mathrm{tg}\,\vartheta_0}{\mathrm{tg}\,\vartheta}\,d\vartheta, \tag{48}$$

on account of (46). This is the "*razor-blade*" case.

A *circular converter* is obtained from the razor-blade shape by putting $c = h$. Then we always have $\vartheta \leqslant \vartheta_0$ and, by (46), Eq. (48) reduces to

$$: \qquad A_\gamma = 2\pi\,K\,\Omega_e \int_0^{\vartheta_0} J(\vartheta+\Delta)\,\mathrm{tg}\,\vartheta\,d\vartheta, \tag{49}$$

which is the case discussed by Hultberg and Stockendal (1959).

It might be observed that, when $\vartheta \to \pi/2$, we have

$$\lim_{\vartheta\to\pi/2} \left(\mathrm{tg}\,\vartheta\;\mathrm{arc\,sin}\,\frac{\mathrm{tg}\,\vartheta_0}{\mathrm{tg}\,\vartheta}\right) = \mathrm{tg}\,\vartheta_0. \tag{50}$$

The integrals (45) and (48) are thus finite and unique. Because $\Delta = \pi/2$ when $\vartheta = \pi/2$, we obtain $J(\vartheta+\Delta) = J(\pi)$.

The practical evaluation of the above integrals is demonstrated in Fig. 13, for the case of a *point source*. The integral expressions (45), (48) and (49) are conveniently obtained from the graph of Fig. 13 by the use of a planimeter. Thus, for a *circular converter* of half top-angle $\vartheta_0$ the integrand ($a$) is followed from $\vartheta = 0$ to $\vartheta = \vartheta_0$. In the case of the *razor-blade shape*, with dimensions defined by

---

[1] In the following formulae we shall, for simplicity, denote the angular function by $J$, no matter whether the numerical values to be substituted for $J$ from Table 2 contain distortions or not.

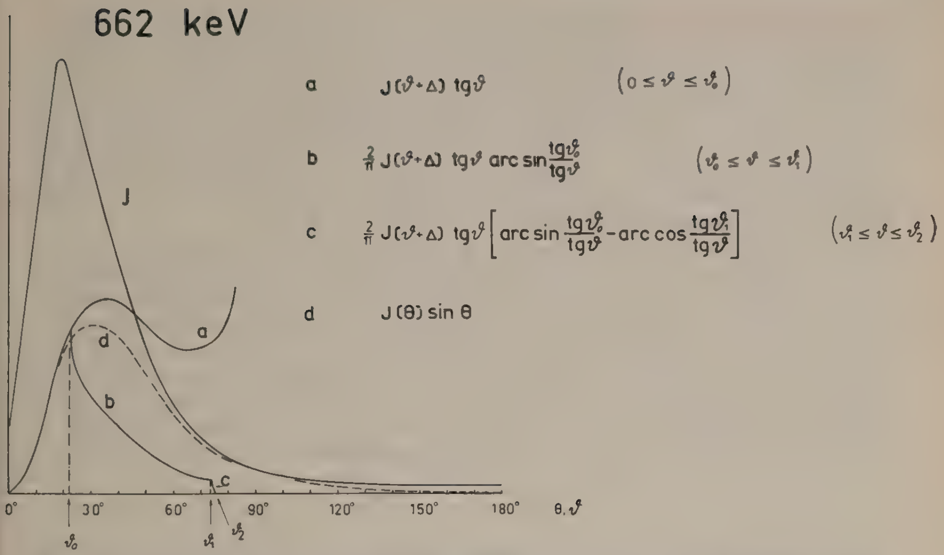

Fig. 13. Illustration of the character of the integrand of formula (45). The diagram applies to a converter with a point source (Fig. 12 *a*). Regarding the factor $2/\pi$, see Eq. (51).

the width $c$ and the half top-angle $\vartheta_1$ the integration is carried out by following curve (*a*) from $\vartheta = 0$ to $\vartheta = \vartheta_0$ and curve (*b*) from $\vartheta = \vartheta_0$ to $\vartheta = \vartheta_1$. The effect of a *rectangular converter*, of width $c$ and height $h$, is obtained from the latter case by adding the integral along (*c*) from $\vartheta = \vartheta_1$ to $\vartheta = \vartheta_2$.

Fig. 12 *b* illustrates the case where the gamma-ray source has finite dimensions. For simplicity, a finite size parallel with the spectrometer axis (the source thickness) is not shown in the figure, but it will be treated below.

### *The case of a source of finite "width"*

Let us consider a *line source* along $P'_Q Q P_Q$, of length $2c_Q$, in the direction of the width dimension of the converter. We then divide the line source into a total number of $2n_c$ point sources which will be equivalent with respect to the height of the converter. For one particular point source, for instance the one at $P_Q$, the normal to the source plane through $P_Q$ intersects the converter at $P_O$. The plane which is normal to the line source and contains $P_Q P_O$ divides the converter into two "real" parts of widths $c \pm c'$ (when $OP_O < c$) and in two "fictitious" parts of widths $c' \pm c$ (when $OP_O > c$), cf. Fig. 12 *b*. The effect of two symmetrically placed point sources $P_Q$ and $P_{Q'}$ is approximately obtained by simply summing the photoelectric contributions (regarded as positive or negative, see below) from two converters, centered at $O$, and of half widths $c_p = c \pm c'$ or $c_p = c' \pm c$, according as $c > c'$ or $c < c'$, respectively. The contribution from each "partial" converter can be calculated from (45), in the manner described above, with $\vartheta_1$ being kept fixed. The approximation of centering all the partial converters at $O$ is good as long as $c_p \ll m$, i.e. when the angle $SP_QP_O$ is small. The *total* effect of the line source will be obtained by summing the photoelectric contributions from the $2n_c$ partial converters and dividing by $2n_c$,[1] under the convention that all integrals resulting from converters of half widths $c_p = c \pm c'$ $(c > c')$ and $c_p = c' + c$ $(c < c')$ be considered as *positive*, while integrals resulting from half widths $c_p = c' - c$ $(c' > c)$ be regarded as *negative*. Here $c$ and $c'$ are always taken to be positive quantities. It is also understood that the *smaller* of the rectangular converter dimensions be considered as *width* and the *larger* dimension as *height*, irrespective of orientation in space.

Our procedure of taking the finite extension of the line source into account is equivalent to a concentration of the $2n_c$ point sources at $Q$ and replacing, at $O$, the converter by a number of $2n_c$ "partial" converters of different widths, representing positive or negative contributions to the total photoelectric intensity. The result can be interpreted as a specific value of the integral (45) if $\vartheta_0$ is suitably chosen (keeping $\vartheta_1$ constant). Thus, we can regard our method as a procedure of reducing the line source to a point source, having the total gamma-ray intensity, and replacing the converter half width $c$ by an *effective half width* $c_e$. This is equivalent to an adjustment of the characteristic angle $\vartheta_0$.

### *The case of a source of finite "height"*

Next we consider a line source along $M_Q Q M'_Q$, of length $2\ h_Q$, in the direction of the height dimension of the converter (Fig. 12 *b*). We divide the line source into a total number of $2n_h$ point sources which will be equivalent with respect to the width of the converter. The straight line through a particular point source $M_Q$ and parallel with the spectrometer axis intersects the converter at $M_O$. Proceeding in a manner quite analogous to that discussed above, we can calculate the photoelectric intensity from the converter, due to the action of the symmetrically situated point sources $M_Q$ and $M'_Q$. It will be obtained as the total contribution from two fictitious converters of the same width $c$, but of half heights $h_p = h \pm h'$ or $h' \pm h$, according as $h > h'$ or $h < h'$, respectively. $h$ and $h'$ are always *positive* quantities. Keeping $\vartheta_0$ fixed, the contributions from the "partial" converters are calculated from (45), where the upper limit $\vartheta_2$ depends on $h_p$. When $h_p < c$ it should be observed that the dimensions $c$ and $h_p$ interchange their roles, so that $c$ now determines the characteristic angle $\vartheta_1$ while $h_p$ gives $\vartheta_0$.[2] Some typical situations in the course of these calculations are shown in Fig. 14 *a–g*. As above, we have made the approximation that $h_p \ll m$, a condition that is generally well fulfilled. The total photoelectric intensity results from the action of all the point sources and is obtained by averaging over all partial contributions, as before. The latter are to be taken with a negative sign when $h_p = h' - h$. The result can be identified with a particular integral (45) if $\vartheta_2$ is suitably chosen. As before, our procedure can be interpreted as concentrating the total gamma-ray intensity at $Q$ and assigning an *effective half height* $h_e$ to the converter. The adjustment of the end-point $\vartheta_2$ of curve (*b*) of Fig. 13 thus represents the effect of the finite height extension of the source.

---

[1] Physically, we regard the $2n_c$ point sources as equally intense, i.e. to each such point is assigned a gamma-ray intensity $I_\gamma k_\gamma/(2n_c)$.

[2] A corresponding interpretation interchange can also take place with $c_p$ and $h$ in the treatment of the source width, if $c_p > h$.

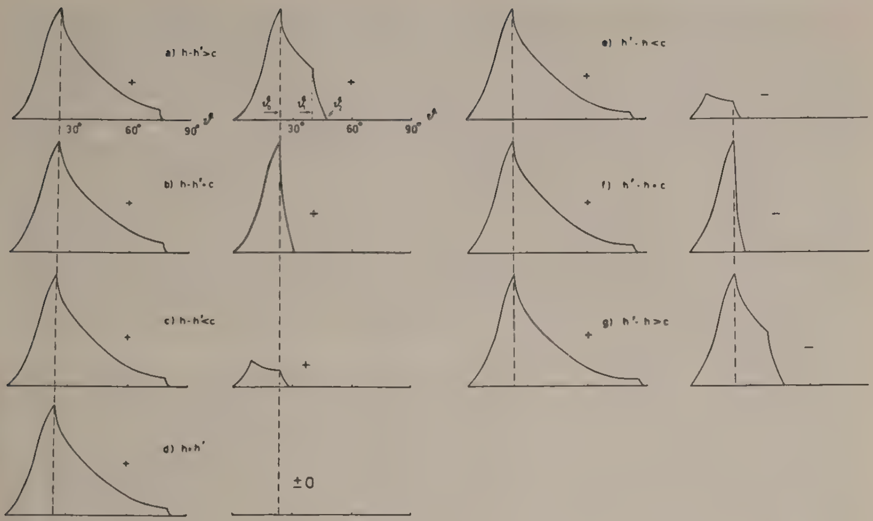

Fig. 14. Illustration of some characteristic steps in the procedure of "reducing" the finite height extension of a gamma-ray source. The contours represent the integrand of Eq. (45) (cf. Fig. 13). The area between each contour and the $\vartheta$-axis should be taken with the sign indicated ($+$ or $-$).

## *The general case*

It is now obvious how we shall treat the general case of a truly rectangular source (Fig. 12 *b*). First we divide the converter in $2n_c$ rectangular parts, each part having a width that is small compared with $c$. Every part is then represented by a line source through its centre and parallel with the height dimension of the converter. In Fig. 12 *b* the dotted line through $P_Q$ represents such a line source. A *first set* of $2n_c$ partial converters is obtained by associating partial converters with the line sources, in the manner described above for the reduction of the source width. Each partial converter should then be treated according with the procedure for the reduction of the source height, implying that with each partial converter of the first set is associated a *second set* of $2n_h$ partial converters. Summing the $4n_c n_h$ partial contributions and dividing by $4n_c n_h$ gives the final value of the integral (45) for the rectangular source.

On account of the similarity of the "contour" curve (*a*)–(*b*) of Fig. 13 for different values of $\vartheta_0$, it is possible in many cases to simplify the preceding method by first forming the resultant contribution from the first set, according to the above treatment of the source width. This means that, for a moment, we neglect that the source has a finite height. The resultant then has the same characteristic angle $\vartheta_1$ as its constituents and it is then possible to identify it with a particular integral (45), by choosing $\vartheta_0$ properly. This first step can be interpreted as a reduction of the rectangular source to a line source through $O$, in the direction of $h$. Secondly, the line source can be treated according to the above method of reducing the source height, giving the final result.

The above complete treatment for an extended and infinitely thin gamma-ray source can obviously be repeated for several values of the source–converter distance $a$. Choosing the step $\Delta a$ such that the variations of $\vartheta_0$ and $\vartheta_1$ over $\Delta a$ are small and taking the arithmetical average of the (positive) partial contributions with respect to $a$, the problem of treating a gamma-ray source of arbitrary dimensions has been completely solved, within the validity of the above-mentioned approximation. In practice, however, the reduction of the source thickness is seldom necessary because, in order to avoid difficult corrections for self-absorption of the quanta inside the source, it is necessary to reduce $d_Q$ as far as possible. This means that taking $\vartheta_0$ and $\vartheta_1$ at the symmetry centre of the source usually gives a very good approximation. However, in cases where the gamma-ray self-absorption is negligible and where intensity requirements are otherwise difficult to meet, thick sources might be used to advantage, if the above treatment is carried out for all three dimensions.

In the above discussions of the finite source dimensions we have, for simplicity, carried out summations over discrete quantities. In practice, however, one should plot the photoelectric contribution due to the action of a specific point source, relative to that of the point source at $Q$, versus its coordinate $c'_Q$ or $h'_Q$ in so-called *efficiency diagrams* (one for each combination of atomic shell and gamma-ray energy), where the ordinate at $c'_Q = h'_Q = 0$ represents a converter efficiency of 100 %. The *efficiency curves* so obtained can then be integrated over the source dimensions (cf. Marklund *et al.*, to be published).

In order to simplify the numerical work necessary for treating the finite source dimensions, the integral occurring in (45) can be evaluated once and for all for a number of combinations of the characteristic angles $\vartheta_0$ and $\vartheta_1$. If the increment $\Delta$ is at first neglected one can conveniently plot the integral (45) as a function of $\vartheta_1$ in a diagram (for a specific shell-energy combination), where a set of curves is then obtained with $\vartheta_0$ as parameter. With help of interpolation such a *key diagram* immediately gives all required values of the integral (45), at a specific energy and for a specific shell. The increment $\Delta$ can be accounted for by multiplying each value of the key diagram with a correction factor which is obtained from a set of curves in a separate $\Delta$-*diagram*, where the correction factor is given as a function of $\vartheta_1$ and where the quantity $a/m$, Eq. (47), is the parameter. With such diagrams at hand a complete treatment of the finite source dimensions for a specific case is a matter of a couple of hours. In order to facilitate the use of our method we plan to make the necessary diagrams directly available from the Nobel Institute, on request.

*The determination of relative gamma-ray intensities, internal conversion coefficients and photoelectric cross-sections.*

For the practical use of Eq. (45) we insert the photoelectric cross-section $\tau$ into (45), by using the definitions (24) and (30)′. We obtain, for a particular shell,

$$\left.\begin{aligned} A_\gamma &= I_\gamma \tau f d k_\gamma b c_\gamma, \\ f &= \frac{\dfrac{2}{\pi}\displaystyle\int_0^{\vartheta_2} J(\vartheta+\Delta)\,\mathrm{tg}\,\vartheta\left(\arcsin\frac{\mathrm{tg}\,\vartheta_0}{\mathrm{tg}\,\vartheta} - \arccos\frac{\mathrm{tg}\,\vartheta_1}{\mathrm{tg}\,\vartheta}\right)d\vartheta}{\displaystyle\int_0^{\pi} J(\theta)\sin\theta\,d\theta}. \end{aligned}\right\} \qquad (51)$$

*Table 2.* Numerical values of the photoelectric angular functions, per unit solid angle, for the $K$, $L$ and $M+N+\cdots$ shells, at three gamma-ray energies. $Z=92$.

The $K$-shell functions represent true distributions $J$ while the functions of the higher shells represent the experimental functions $J_e$ of Fig. 5. For each energy, the three functions given are mutually correct on a relative scale, so that $K/L$, $K/(M+N+\cdots)$ and $L/(M+N+\cdots)$ ratios in external conversion can be calculated.

| $\theta°$ | $h\nu=412$ keV | | | $h\nu=662$ keV | | | $h\nu=1332$ keV | | |
|---|---|---|---|---|---|---|---|---|---|
| | $K$ | $L$ | $M+N+\cdots$ | $K$ | $L$ | $M+N+\cdots$ | $K$ | $L$ | $M+N+\cdots$ |
| 0 | 37 | 89 | 27 | 49 | 97 | 32 | 111 | 96 | 32 |
| 3 | 72 | 89 | 27 | 114 | 97 | 32 | 196 | 96 | 32 |
| 6 | 112 | 89 | 27 | 177 | 97 | 32 | 281 | 93 | 31 |
| 9 | 150 | 90 | 27 | 240 | 96 | 32 | 363 | 87 | 30 |
| 12 | 190 | 90 | 27 | 303 | 94 | 32 | 409 | 78 | 27 |
| 15 | 229 | 91 | 28 | 366 | 92 | 31 | 365 | 68 | 24 |
| 18 | 267 | 90 | 28 | 409 | 89 | 31 | 317 | 59 | 22 |
| 21 | 307 | 89 | 28 | 401 | 84 | 30 | 270 | 50 | 19 |
| 24 | 346 | 87 | 29 | 370 | 78 | 28 | 221 | 40 | 16 |
| 27 | 385 | 83 | 29 | 339 | 70 | 27 | 173 | 32 | 13 |
| 30 | 410 | 79 | 29 | 308 | 63 | 25 | 125 | 24 | 11 |
| 33 | 397 | 75 | 29 | 278 | 55 | 24 | 87 | 18 | 8 |
| 36 | 376 | 70 | 29 | 250 | 49 | 21 | 64 | 13 | 6 |
| 39 | 355 | 66 | 28 | 223 | 43 | 19 | 47 | 10 | 4 |
| 42 | 334 | 62 | 27 | 197 | 36 | 17 | 34 | 7 | 3 |
| 45 | 313 | 58 | 25 | 174 | 31 | 15 | 27 | 6 | 2 |
| 48 | 292 | 54 | 23 | 150 | 26 | 13 | 22 | 5 | 1 |
| 51 | 271 | 49 | 22 | 128 | 23 | 11 | 18 | 4 | 1 |
| 55 | 243 | 44 | 19 | 105 | 19 | 8 | 15 | 2 | 0 |
| 60 | 208 | 37 | 16 | 82 | 14 | 6 | 11 | 0 | |
| 65 | 174 | 31 | 13 | 65 | 11 | 4 | 8 | | |
| 70 | 147 | 26 | 11 | 52 | 9 | 2 | 6 | | |
| 75 | 125 | 21 | 9 | 42 | 6 | 1 | 4 | | |
| 80 | 106 | 18 | 7 | 32 | 5 | 1 | 2 | | |
| 85 | 91 | 15 | 5 | 26 | 4 | 0 | 1 | | |
| 90 | 78 | 12 | 4 | 22 | 3 | | 0 | | |
| 100 | 60 | 8 | 3 | 16 | 1 | | | | |
| 110 | 48 | 6 | 2 | 13 | 0 | | | | |
| 120 | 38 | 4 | 1 | 10 | | | | | |
| 130 | 30 | 2 | 1 | 9 | | | | | |
| 140 | 24 | 1 | 0 | 8 | | | | | |
| 150 | 20 | 1 | | 7 | | | | | |
| 160 | 17 | 0 | | 6 | | | | | |
| 170 | 15 | | | 6 | | | | | |
| 180 | 14 | | | 6 | | | | | |

where $\vartheta_0$, $\vartheta_1$ and $\vartheta_2$ now refer to the *reduced* converter dimensions, introduced above. In (51) the baffle solid angle $\Omega_e$ has been replaced by the spectrometer transmission factor $c_\gamma$. The supplementary conditions (46) and (47) are to be observed when evaluating (51). For the special cases of the razor-blade shape or the circular shape, the numerator integrand of (51) reduces to that of (48) or (49), respectively. For the use of (51) in the determination of *relative gamma-ray intensities*, the quantities $d$, $k_\gamma$, $b$ and $c_\gamma$ are kept constant and in order to obtain $I_\gamma$ it is only necessary to divide the observed photoline intensities $A_\gamma$ by the appropiate value of $\tau f$. The *internal conversion process*, being assumed isotropic, gives for

*Table 3.* $K$-shell photoelectric cross-sections for uranium (White, 1957). $\tau_K$ is given in barns/atom and the gamma-ray energy in MeV. The accuracy of the $\tau_K$ values is discussed in section G.

| $h\nu$ | $\tau_K$ | $h\nu$ | $\tau_K$ |
|---|---|---|---|
| 0.116 | 1535 | 0.80 | 14.1 |
| 0.15 | 786 | 1.0 | 9.2 |
| 0.20 | 364 | 1.5 | 4.5 |
| 0.30 | 125 | 2.0 | 2.9 |
| 0.40 | 64.4 | 3.0 | 1.7 |
| 0.50 | 37.9 | 4.0 | 1.1 |
| 0.60 | 25.7 | 5.0 | 0.9 |

the recorded intensity, using a separate source,

$$A_\beta = I_\beta k_\beta c_\beta,$$

where the quantities introduced have definitions analogous to those of Eq. (51). Combining with (51) we obtain for the *absolute value* $\varepsilon$ of the internal conversion coefficient $(k = k_\gamma / k_\beta)$

$$\varepsilon = \frac{A_\beta}{A_\gamma} \tau f d k b, \tag{52}$$

where $c_\beta = c_\gamma$ is assumed. The expression (52) and its use for the case of cylindrical symmetry around the spectrometer axis was discussed by Hultberg and Stockendal (1959 *a*). With Eq. (52) *absolute values of* $\tau$ can be obtained from studies of transitions where $\varepsilon$ can be considered to be accurately known (Hultberg and Stockendal, 1959 *b*).

For the use of Eqs. (51) and (52) the correction factor $f$ is evaluated according to the above discussion of the source–converter geometry, with due regard being paid to the finite source dimensions. In order to be specific, it might be pointed out that when $c_Q < \frac{1}{2} c$ and $h_Q < \frac{1}{2} h$ the effect of the source size can be neglected to a good approximation (to better than 1 % at 400 keV and above, and to better than 5 % at the $K$-edge). It should be observed that our formulae are valid only for the case of a central aperture, as is the case for flat spectrometers. Of course, the angular functions can be applied to helical spectrometers as well, if the more complicated integration over the ring baffle is carried out (cf. Thomas, 1952). Because of the higher luminosity of the latter type of instrument, it would be highly desirable that an attempt in this direction be made. Our Eq. (51) should then obtain as a limiting case.

In order to render the expressions (51) and (52) universally accessible we present, in Table 2, our angular functions in numerical form. For the sake of completeness we give, in Table 3, the $K$-shell photoelectric cross-sections $\tau_K$, as obtained from the tables of White (1957) by removing the $\tau_{K+L+M}/\tau_K$ factor contained in the tabulated values.

### *Formulae (51) and (52) in practice*

In the present sub-section we shall discuss the practical use of the expressions (51) and (52), and some special tests, performed in order to verify the functional dependence of the correction factor $f$.

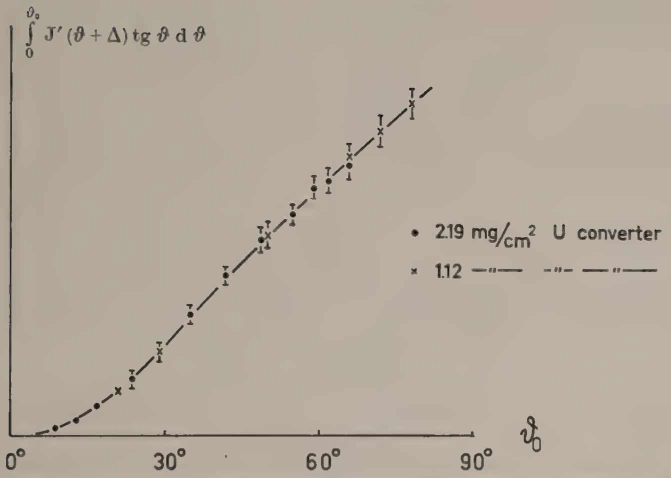

Fig. 15. A test of Eq. (51), for the case of a circular converter and a point source. The experimental points give $A_\gamma(\vartheta_0)$, as a function of $\vartheta_0$, while the full-drawn curve represents the evaluation of (51) by performing the integration over $J_K$, obtained from Table 2. $h\nu = 662$ keV.

Eq. (51) gives the recorded photoelectric intensity for the special case when the gamma-ray source takes the position $\theta = 0$, which is always used in practice. The functional dependence of $f$ can obviously be tested by recording $A_\gamma$ at different source–converter distances $a$. Then all quantities in Eqs. (51) are kept constant, except the upper limit $\vartheta_2$ of the numerator integral of $f$. Such tests were carried out for the three $K$-shell functions of Table 2, for the case of a circular converter. The result at $h\nu = 662$ keV is shown in Fig. 15. The proportionality factor between the recorded intensities and the corresponding ordinates of the full-drawn curve of Fig. 15 was constant in the whole angular interval covered by the experiments. The agreement was found to be equally good at the two other energies.

Considering the exact character of the angular function $J$ to be used in calculating the ordinates of Fig. 15, it is possible, by use of Fig. 7 and the condition (38), to construct a function $J' = J'(\vartheta_0 = 0;\ d \neq 0)$ with the correct information about the scattering. However, as is seen from Fig. 15, the practical difference is negligible. This fact can be readily understood by considering that the difference $\delta J$ in the shapes of $J$ and $J'$ is appreciable only at small angles. Moreover, $\delta J$ has opposite signs at $\theta = 0$ and at $\theta = \theta_m$, implying that $\delta J = 0$ somewhere in between. The multiplication by the sine and tg functions further reduces $\delta J$ at small angles. We assume, throughout, that the converter material is thin enough, so that all absorption processes of the photoelectrons in the converter material can be disregarded.

From Fig. 13 it can be seen that often the rectangular converter shape is to be preferred, because (*a*) it will not accentuate the low parts of $J$ as much as will the circular shape, (*b*) it often spans a very large angular interval of $J$, implying that the "cancelling effects" on $\delta J$ are better used, and (*c*) it permits

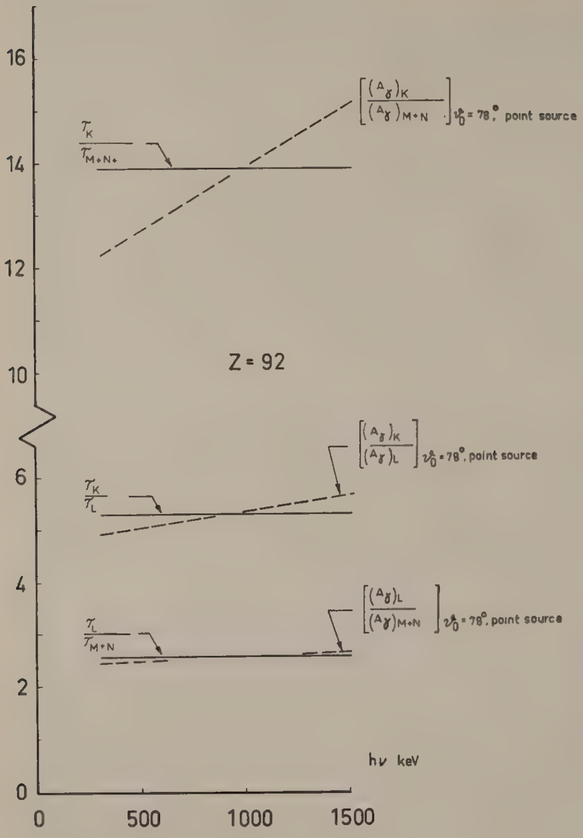

Fig. 16. The full-drawn lines give photoelectric absorption ratios for the uranium atom, as calculated from Eq. (41). The dotted lines represent photoline ratios for a circular converter and a point source with $\vartheta_0 = 78°$, as computed from Eq. (51).

a better instrumental resolution. A disadvantage lies in the circumstance that two angular limits, $\vartheta_0$ and $\vartheta_1$, have to be determined. Which converter shape that is to be preferred must be decided in each particular case.

Formula (51) was also tested for rectangular converters by recording photolines, using the converter dimensions $3 \times 20$, $5 \times 20$ and $13 \times 20$ mm$^2$ (keeping $a$ constant). The ratios obtained from calculations of the corresponding integrals were in good agreement with the experimental ratios. The source was small enough to neglect the effect of its finite size. In order to test the above introduced "method of partial converters", we measured photolines, using a $6 \times 6$ mm$^2$ electroplated Co$^{60}$ source, together with converters of dimensions $13 \times 20$ and $2 \times 20$ mm$^2$ ($a = 2$ mm). In the former case the source size is effectively negligible ($c_Q < \frac{1}{2} c$, cf. above), but in the latter we have $c_Q = 3\ c$ (cf. Fig. 12b). Since $h_Q \ll h$ the source could in both cases be regarded as a line source, in the direction of the converter width. The calculated ratio of the photolines (0.32) agreed with the experimentally found ratio (0.32). With the $2 \times 20$ mm$^2$ converter and $6 \times 6$ mm$^2$ source we also performed a special test by moving the converter in the direction of its width (i.e. moving it on the spectrometer radius). It was then found that the exact position of the converter on the spectrometer radius was not critical within ±1 mm. This is due to averaging effects over the angular functions. The same will also be true in the reverse case, i.e. when the source is smaller than the converter. In cases where it is difficult to establish the correct radial position, it is recommended to find the latter by recording the intensity at the photoline peak, for a few radial positions. Similar considerations will apply to the adjustment in the height direction.

Finally, the above procedure for taking the finite source height into account was tested by moving a point source along $QM_Q$ (Fig. 12b). Photolines were recorded for a few positions of $M_Q$, corresponding to $h' < h$, $h' = h$ and $h' > h$ (cf. Fig. 14). The expected intensity ratios were calculated from the corresponding set of partial converters, and the result was again found to agree well with experiment.

We thus conclude that our approximation of neglecting the dimensions of the source–converter geometry in comparison with the distance $m$ to the baffle centre $S$ is justified. Also, on the basis of the experimental tests, we consider our "method of partial converters" adequate for dealing with any source–converter geometry of practical interest to a sufficient degree of accuracy. The latter statement means that the contribution from the factor $f$ to the total error, connected with the use of Eqs. (51) and (52), should in most cases be less than 5%. This is partly due to the fact that $f$ is formed as a ratio between two integrals over the same function. Thus there is a strong tendency that an error $\delta J$ in $J$ (contained in an approximation, for instance) will cancel out in $f$. We may then expect that the exact shape of the angular functions to be used in practice should not be too critical. The latter statement means that even *uncorrected* experimental functions can be used in the above formulae (cf. Hultberg and Stockendal, 1959 *a*). Even for the full-drawn curve of Fig. 15 no significant difference was obtained between calculations based on functions, containing different amounts of distortion. Since no extrapolation measurements were carried out for the higher atomic shells and since the method for solving Eq. (35) is the object of extended work (Rådström and Philip, cf. p. 329) we prefer to present our *experimental* functions $J_e$ for the $L$ and $M+N+\cdots$ shells. According to the above discussion no appreciable errors should be introduced by their use (as before, the associated errors probably do not exceed 5%).

By using (51) on the different functions of Table 2, it is possible to calculate $K/L$, $K/(M+N+\cdots)$ and $L/(M+N+\cdots)$ ratios in external conversion for the particular geometry. This is of special value in cases of complex spectra (see next section). Such calculations were found to agree with experiment in cases where $K$, $L$ and $M+N+\cdots$ lines were resolved. An illustration is given in Fig. 16.

## I. Remarks and conclusions

In the preceding sections we have described a series of measurements, leading to an experimental representation of the longitudinal photoelectric angular distribution. We have discussed the properties of our curves and of available theory, and we have indicated their usefulness. In the present section we shall add some concluding remarks.

We would like to point out here that, for small gamma-ray energies, it may sometimes be advantageous to use the photoelectric conversion in the $L$ and $M+N+\cdots$ shells. At photon energies above the $K$-shell binding energy, Eqs. (41) and (51) combine into

$$(A_\gamma)_L = I_\gamma \tau_K d\, k_\gamma b\, c_\gamma \frac{\frac{2}{\pi}\int\limits_0^{\vartheta_2} J_L(\vartheta+\Delta)\operatorname{tg}\vartheta\left(\operatorname{arc\,sin}\frac{\operatorname{tg}\vartheta_0}{\operatorname{tg}\vartheta} - \operatorname{arc\,cos}\frac{\operatorname{tg}\vartheta_1}{\operatorname{tg}\vartheta}\right)d\vartheta}{\int\limits_0^{\pi} J_K(\theta)\sin\theta\, d\theta} \tag{53}$$

where $J_L$ and $J_K$ are obtained from Table 2. Replacing the index $L$ by $M+N+\cdots$ we obtain an analogous expression for the $M+N+\cdots$ shell conversion. At quantum energies below 116 keV, Eq. (51) has to be used.

If great care is taken in the mounting of the gamma-ray source and the converter, the characteristic angles can be accurately determined and it should be possible to reach an accuracy in the factor $f$ of 1–3%. The latter figure represents a residual error which is difficult to estimate since it depends on the shape of the angular functions for angles above $\theta = 90°$. From our experience so far it is, however, felt that such an estimate is quite reasonable. As soon as reliable theoretical values of $J(\theta)$ become available it will be easier to judge the real accuracy.

Except in particularly favourable cases, the accuracy of the measured photoline intensities usually determines the final error in $I_\gamma$ and $\varepsilon$, evaluated according to (51) and (52). In this connection we should like to stress that the importance of exercising the utmost care in the recording of the continuum on both sides of a photoline cannot be overestimated. For the accurate evaluation of the intensity of a photoline it seems well to recommend measuring a total $H\varrho$ region (with the line peak at the centre), spanning at least 10 times the total width at half maximum of the photopeak. If there is more than one photoline in such a region, or/and if the intensity is very low, the $H\varrho$ region should be correspondingly extended. Following such a convention it is possible to reach a good reproducibility in the measurements.

In our experiments we have used uranium converters exclusively, because it is relatively easy to obtain a high uniformity in their preparation. By applying (51) and/or (53) to photoelectric conversion in higher atomic shells, the drawback of the high $K$-shell binding energy of uranium is removed, and, by employing a number of uranium converters of various thicknesses, it seems that this element is well suited for external conversion work.

The present paper is intended to report our experiences gained so far. It is hoped that it will contribute to a stimulation towards a more general use of photoelectric conversion for the determination of relative gamma-ray intensities and absolute internal conversion coefficients (or of absolute photoelectric cross-sections, cf. Hultberg and Stockendal, 1959*a*, *b*). Apart from the attainable precision and experimental simplicity the greatest advantage of our method is perhaps that the resulting $I_\gamma$ and $\varepsilon$ do not depend on any previously acquired information on the actual or on other decay schemes, in contrast to other methods. Measurements based on Eqs.

(51) and (52) can thus be said to be completely "self-consistent", in that only one instrument is used and no previous information of any kind is required. However, some useful work on the photoelectric effect of methodical character still remains. For various reasons it may be desirable to use converter materials other than uranium (copper, silver, gold, platinum, lead, bismuth, etc.), and it would be of interest to make a closer study of the $Z$-dependence of the angular functions, as well as of the angular distributions for uranium outside the energy interval, covered by the present experiments.[1] Because of the higher luminosity of helical spectrometers it would be of importance to extend the treatment of the source–converter geometry to the case of a ring baffle (cf. section H). A great achievement would also be made if the troublesome Compton background could be eliminated (cf. *Note added in proof*).

Theoretically, it seems highly desirable that an effort be made towards a systematic computation of really accurate photoelectric cross-sections for the $K$-shell. Using experimental $\tau_a/\tau_K$ ratios (cf. section G, for U), a *true* comparison could then be made with data from absorption measurements. As indicated in section G we should obtain better possibilities of checking the pair production process after having established the validity of available photoelectric cross-sections.

*Note added in proof.*—Experiments have very recently been performed by B. Johansson and R. Stockendal with the purpose to lower the Compton-background in external conversion measurements. A thin scintillator and a light-guide were placed between the converter and the source and mounted on a photomultiplier tube. Using anticoincidence techniques a decrease with, in some cases, 70% of the background was observed, while the photoline intensity remained the same. The experiments are being continued and the results will be published later.

## SUMMARY

A beta-spectrometric study of the longitudinal angular dependence (the $\theta$-dependence) of the photoelectric effect is reported. The $K$, $L$, and $M+N+\cdots$ shells of the uranium atom have been studied in the complete angular interval $0 \leqslant \theta \leqslant \pi$, at the gamma-ray energies 412, 662, and 1332 keV. The influence on the distributions from the set-up geometry and the scattering is discussed. By carrying out special experiments and performing numerical calculations, using a fast electronic computor, the distorting effects could be partly corrected for. The experimental distributions are compared with available theoretical expressions, and the usefulness of the angular functions for ($a$) the study of relative gamma-ray intensities, ($b$) the determination of *absolute* internal conversion coefficients, and ($c$) the *absolute* measurement of photoelectric cross-sections is discussed. The absorption ratios $79.5 \pm 0.6$ % ($K$-shell), $14.8 \pm 0.5$ % ($L$-shell), and $5.7 \pm 0.3$ % ($M+N+\cdots$ shells) were found for the uranium atom, independently of energy, giving $\tau_a/\tau_K = 1.26 \pm 0.02$. The accuracy of available photoelectric cross-sections is discussed and is considered to be about 5 %. Practical formulae are given for the correct deduction of gamma-ray intensities from photolines. For the latter purpose the measured angular functions are given numerically in a table, for all angles $\theta$. The case of rectangular shapes of the gamma-ray source and the converter is considered, with no restrictions being imposed on the relative dimensions, i. e. the source may even be larger than the converter. The latter generalization is valid inside an approximation that is fulfilled in most practical cases. Apart from the errors in the evaluation of the photoline intensities and in available $\tau_K$-values the application of the

---

[1] Z. Sujkowski has recently studied the $\theta$-function for the uranium $K$-shell at a gamma-ray energy of 2.6 MeV (to be published).

present techique to the analysis of photolines is expected to be accurate to within 1–5 %, depending on the geometry and the accuracy in the determination of certain parameters. The method for taking the finite dimensions of the source–converter geometry into account has been tested experimentally and was found to be satisfactory. From the tabulated angular functions, $K/L$, $K/(M+N+\cdots)$ and $L/(M+N+\cdots)$ ratios for external conversion in uranium can be obtained for any practical source–converter geometry.

## ACKNOWLEDGEMENTS

The author wishes to thank Drs. G. Dahlquist, B. Nagel, P. O. Olsson, and H. Rådström, Stockholm, for many helpful discussions and valuable criticism. I am indebted to the Swedish Board for Computing Machinery for putting machine time at my disposal, free of charge, and to the technical staff of the electronic computor BESK for invaluable help. Thanks are also due to Dr. I. Marklund, Uppsala, for stimulating my interest in generalizing the method of the analysis of photolines to the case of rectangular converters.

*Nobel Institute of Pysics, Stockholm 50.*

## REFERENCES

BANERJEE, H., On Sommerfeld's approximation in high energy photoelectric effect and one quantum annihilation of positrons in the $K$-shell. Il Nuovo Cimento *X*, 863 (1958).

BECKER, R., Theorie der Elektrizität II. B. G. Teubner, Leipzig 1949.

COLGATE, S. A., Gamma-ray absorption measurements. Phys. Rev. *87*, 592 (1952).

DAVISSON, C. M., Interaction of gamma-radiation with matter. Beta- and gamma-ray spectroscopy (editor K. SIEGBAHN), 24. North-Holland Publ. Comp., Amsterdam, 1955.

DAVISSON, C. M., and EVANS, R. D., Gamma-ray absorption coefficients. Revs. Mod. Phys. *24*, 79 (1952).

EGGLESTON, F. F. H., and MARTIN, L. H., The angular distribution of photoelectrons from the $K$-shell. Proc. Roy. Soc. *A 162*, 95 (1937).

FISCHER, J., Beiträge zur Theorie der Absorption von Röntgenstrahlen. Ann. Phys. *8*, 821 (1931).

GLOVER, K. M., and BORRELL, P., A method for the preparation of thin films of plutonium and uranium. J. Nuclear Energy *1*, 214 (1955).

GRIGORYEV, E. P., and ZOLOTAVIN, A. V., On the relative probabilities for the photoeffect in shells and subshells of an atom. J. Exp. Theor. Phys. USSR *36*, 393 (1959).

HALL, H., The theory of photoelectric absorption for X-rays and gamma-rays. Revs. Mod. Phys. *8*, 358 (1936).

—— Note on the relativistic formula for photoelectric absorption. Phys. Rev. *84*, 167 (1951).

HEDGRAN, A., Precision measurements of nuclear gamma-radiation by techniques of beta-spectroscopy. Arkiv för Fysik *5*, 1 (1952).

HEDGRAN, A., and HULTBERG, S., Angular distribution of photoelectrons from gamma radiation of 0.4 and 1.3 MeV. Phys. Rev. *94*, 498 (1954).

HEITLER, W., The Quantum Theory of Radiation, 3rd ed. Oxford, 1954.

HEREFORD, F. L., The angular correlation of photoelectrons ejected by annihilation quanta. Phys. Rev. *81*, 482 (1951).

—— The directional distribution of photoelectrons ejected by polarized quanta. Phys. Rev. *81*, 627 (1951).

HEREFORD, F. L., and KEUPER, J. P., The azimuthal distribution of photoelectrons produced by 0.5 MeV polarized photons. Phys. Rev. *90*, 1043 (1953).

HULTBERG, S., An investigation of the longitudinal angular distribution of photoelectrons at gamma-ray energies of 0.41, 0.66, and 1.33 MeV. Arkiv för Fysik *9*, 245 (1955).

HULTBERG, S., and NOVAKOV, T., The longitudinal angular dependence of the photoelectric effect and its influence on the determination of gamma-ray intensities. Nuclear Physics *4*, 120 (1957).

HULTBERG, S., and STOCKENDAL, R., (*a*) On the determination of absolute internal conversion coefficients by the comparison of conversion lines and photolines. An application to the 662 keV transition in the decay of $Cs^{137}$. Arkiv för Fysik *14*, 565 (1959).

—— (*b*) Absolute determinations of *K*-shell photoelectric cross-sections for uranium at the gamma-ray energies 1172 and 1332 keV. Arkiv för Fysik *15*, 355 (1959).

KIRCHNER, F., Allgemeine Physik der Röntgenstrahlen, 164. Handbuch der Experimentalphysik XXIV : 1, Akademische Verlagsgesellschaft, Leipzig, 1930.

LATYSHEV, G. D., The interaction of gamma-rays with matter and the spectroscopy of gamma-radiation. Revs. Mod. Phys. *19*, 132 (1947).

MOLIÈRE, G., Theorie der Streuung schneller geladenener Teilchen II: Mehrfach- und Vielfachstreuung. Zeits. Naturforschung *3 A*, 78 (1948).

NATHAN, O., and HULTBERG, S., Measurements of the gamma-radiations from $Eu^{152}$ by the method of external conversion. Nuclear Physics *9* (1959).

NOVAKOV, T., HULTBERG, S., and ANDERSSON B., A study of the gamma-rays of $Pb^{206}$ from the decay of $Bi^{206}$ by the method of external conversion in uranium. Arkiv för Fysik *13*, 117 (1958).

SAUTER, F., Über den automaren Photoeffekt in der *K*-Schale nach der relativistischen Wellenmechanik Diracs. Ann. Phys. *11*, 454 (1931).

SAUTER, F., and WÜSTER, H. O., Die Emission von Photoelektronen aus der *K*-Schale in Richtung der auslösenden Gamma-Strahlung. Zeits. für Physik *141*, 83 (1955).

SCHIFF, L. I., Quantum Mechanics, 1st ed. McGraw-Hill Book Co., 1949.

SOMMERFELD, A., Atombau und Spektrallinien II, 436, 2nd ed. F. Vieweg & Sohn, Braunschweig, 1939.

SOMMERFELD, A., and SCHUR, G., Über den Photoeffekt in der *K*-Schale der Atome, insbesondere über die Voreilung der Photoelektronen. Ann. Phys. *4*, 409 (1930).

STOCKENDAL, R., and HULTBERG, S., A study of internal conversion coefficients of transitions in $Pb^{205}$ and $Pb^{206}$. Arkiv för Fysik *15*, 33 (1959).

THOMAS, R. G., 1. Spectrometer measurements of the rates of gamma-radiation and internal pair formation from some nuclear reactions in light nuclei. Thesis, Californa Institute of Technology, Pasadena, California (unpublished), 1951.

THOMAS, R. G., and LAURITSEN, T., Magnetic lens spectrometer measurements of the radiations from light nuclear reactions. Phys. Rev. *88*, 969 (1952).

TITUS, F., The photoelectric cross-section at 662 keV. Bull. Am. Phys. Soc. *4*, 269 (1958).

WATSON, E. C., The velocity and number of the photoelectrons ejected by *X*-rays as a function of the angle of emission. Phys. Rev. *30*, 479 (1927).

WATSON, E. C., and VAN DEN AKKER, J. A., Differences in the directions of ejection of X-ray photoelectrons from various atomic levels. Proc. Roy. Soc. *A 126*, 138 (1930).

WHITE GRODSTEIN, G., X-ray attenuation coefficients from 10 keV to 100 MeV. National Bureau of Standards Circular No. 583, April 30, 1957.

Tryckt den 23 april 1959

Uppsala 1959. Almqvist & Wiksells Boktryckeri AB